

1 **~~Unheralded~~Underappreciated contributions of biogenic volatile organic compounds**  
2 **from urban greening to ozone pollution: a high-resolution modeling study**

3  
4 Haofan Wang<sup>1,2,3,4</sup>, Yuejin Li<sup>1,2,3</sup>, Yiming Liu<sup>1,2,3\*</sup>, Xiao Lu<sup>1,2,3</sup>, Yang Zhang<sup>5</sup>, Qi Fan<sup>1,2,3\*</sup>, Chong Shen<sup>6</sup>,  
5 Senchao Lai<sup>7</sup>, Yan Zhou<sup>7</sup>, Tao Zhang<sup>7</sup>, Dingli Yue<sup>7</sup>

6  
7 <sup>1</sup>*School of Atmospheric Sciences, Sun Yat-sen University, and Southern Marine Science and Engineering Guangdong Laboratory*  
8 *(Zhuhai), Zhuhai, 519082, ~~PRP~~. R. China*

9 <sup>2</sup>*Guangdong Provincial Field Observation and Research Station for Climate Environment and Air Quality Change in the Pearl*  
10 *River Estuary, Guangzhou, 510275, ~~PRP~~. R. China*

11 <sup>3</sup>*Guangdong Province Key Laboratory for Climate Change and Natural Disaster Studies, Sun Yat-sen University, ~~Zhuhai~~, ~~PRP~~. R.*  
12 *China*

13 <sup>4</sup>*Centre for Atmospheric Science, Department of Earth and Environmental Sciences, ~~The~~ University of Manchester, Manchester,*  
14 *United Kingdom*

15 <sup>5</sup>*College of Resources and Environment, Chengdu University of Information Technology, Chengdu, Sichuan, China*

16 <sup>6</sup>*Guangzhou Climate and Agrometeorology Center, Guangzhou 511430, China*

17  
18 <sup>7</sup>*National Key Laboratory for Regional Air Quality Monitoring of Environmental Protection/Guangdong Ecological Environment*  
19 *Monitoring Center, Guangzhou 510308, P. R. China*

20  
21 *Correspondence to: Yiming Liu ([liuym88@mail.sysu.edu.cn](mailto:liuym88@mail.sysu.edu.cn)), Qi Fan ([eesfq@mail.sysu.edu.cn](mailto:eesfq@mail.sysu.edu.cn))*  
22

## Abstract

Urban Green Spaces (UGS), such as parks and gardens, are widely promoted as a strategy for mitigating the urban atmospheric environment and environmental health. However, this study reveals that it can exacerbate urban ozone (O<sub>3</sub>) levels under certain conditions, as demonstrated by a September 2017 study in Guangzhou, China. Utilizing the Weather Research and Forecasting Model with the Model of Emissions of Gases and Aerosols from Nature (WRF-MEGAN) and the Community Multiscale Air Quality (CMAQ) model with a high horizontal resolution (1 km), we assessed the impact of UGS-related biogenic volatile organic compound (BVOC) emissions on urban O<sub>3</sub>. Our findings indicate that the UGS-BVOC emissions in Guangzhou amounted to 666.49 Gg, primarily from (~90 Mg/km<sup>2</sup>), with isoprene (ISOP) and terpenes/monoterpene (TERP). These contributing remarkably to the total UGS-BVOC emissions contribute ~30% of urban ISOP concentrations. In comparison to anthropogenic VOC (AVOC) and their incorporations to the BVOC emissions, UGS-BVOC emissions account for approximately 33.45% in the city center region. Incorporating UGS-BVOC emissions into the model significantly reduces the underestimation against of ISOP levels compared to observations. The study shows improvements in simulation biases for NO<sub>2</sub>, from 7.01 μg/m<sup>3</sup> to 6.03 μg/m<sup>3</sup>, and for O<sub>3</sub>, from 7.77 μg/m<sup>3</sup> to -1.60 μg/m<sup>3</sup>. UGS-BVOC and UGS-LUCC (land use cover changes) integration in the air quality models notably enhances surface monthly mean O<sub>3</sub> predictions by 1.7-3.6 μg/m<sup>3</sup> and contributes up to 18.7 μg/m<sup>3</sup> to MDA8 O<sub>3</sub> during O<sub>3</sub> pollution episodes. Additionally, UGS-BVOC emissions alone increase the monthly mean O<sub>3</sub> levels by 2.2-3.1 μg/m<sup>3</sup> in urban areas and contribute up to 6.3 μg/m<sup>3</sup> to MDA8 O<sub>3</sub> levels during O<sub>3</sub> pollution episodes. These impacts can extend to surrounding suburban and rural areas through regional transport, highlighting the need for selecting low-emission vegetation and refining vegetation classification in urban planning. The importance of accurately accounting for UGS-BVOC emissions to better understand and manage their impact on regional air quality.

## Keywords

Urban green space; BVOC; Ozone; Land use cover; CMAQ; MEGAN

## 1. Introduction

Exposure to air pollution now accounts for more fatalities than malaria, tuberculosis, and HIV/AIDS combined (Lelieveld et al., 2020). As a result, the World Health Organization has declared air pollution the most significant environmental threat to human health (WHO, 2021). Notably, over 70% global health burden of air pollution stems from human-made emissions, leading to a policy focus predominantly on reducing these emissions (Chowdhury et al., 2022; Lelieveld et al., 2019). Despite proactive measures to curb anthropogenic emissions, the incidence of ozone episodes is escalating alongside rapid urbanization (Lu et al., 2020; Yim et al., 2019). Numerous studies have investigated the effects of land use cover changes (LUCC) on air quality during urbanization using numerical models and the majority of these studies conclude that urbanization exacerbates air pollution (Qiu et al., 2023; Wang et al., 2022). However, such studies that depend on numerical models usually face the coarse resolution land use cover data limitation (Ma et al., 2022, 2019), which leads these studies to frequently overlook a passive abatement approach distinct from reducing anthropogenic sources—namely, the cultivation of urban green spaces (UGS) (Cohen et al., 2017).

The widely accepted notion that UGS can enhance air quality is substantiated by various strands of literature, including public health (Burnett et al., 2018), urban planning (Solomon, 2007), and ecosystem services (Lohmann et al., 2010). This concept is not only prevalent in scholarly circles but also gains traction in popular media and is echoed in international standards and policy frameworks. For instance, the United Nations System of Environmental Economic Accounting advocates for vegetation as a nature-based approach to mitigate air pollution (Le Page et al., 2015). Vegetation primarily contributes to air pollution reduction through two mechanisms: deposition and dispersion (Shindell et al., 2012). Deposition involves the absorption of air pollutants onto vegetative surfaces, while dispersion refers to the reduction of air pollutant concentrations through aerodynamic effects caused by vegetation (Zhao et al., 2022). Notably, dispersion effects are significantly more impactful than deposition, exceeding it by an order of magnitude (Ramanathan et al., 2001). Exposure to air pollution now accounts for more fatalities than malaria, tuberculosis, and HIV/AIDS combined (Lelieveld et al., 2020). As a result, the World Health Organization has declared air pollution the most significant environmental threat to human health (WHO, 2021). Notably, over 70% global health burden of air pollution stems from human-made emissions, leading to a policy focus predominantly on reducing these emissions (Chowdhury et al., 2022; Lelieveld et al., 2019). Despite proactive measures to curb anthropogenic

79 emissions, the incidence of ozone episodes is escalating alongside rapid urbanization (Lu et al., 2020; Yim et  
80 al., 2019). Numerous studies have investigated the effects of land use cover changes (LUCC) on air quality  
81 during urbanization using numerical models and the majority of these studies conclude that urbanization  
82 exacerbates air pollution (Qiu et al., 2023; Wang et al., 2022). However, such studies that depend on numerical  
83 models usually face the coarse-resolution land use cover data limitation (Ma et al., 2022, 2019), which leads  
84 these studies to frequently overlook a passive abatement approach distinct from reducing anthropogenic  
85 sources—namely, the cultivation of urban green spaces (UGS) (Cohen et al., 2017).

87 The widely accepted notion that UGS can enhance air quality is substantiated by various strands of literature,  
88 including public health (Burnett et al., 2018), urban planning (Solomon, 2007), and ecosystem services  
89 (Lohmann et al., 2010). This concept is not only prevalent in scholarly circles but also gains traction in popular  
90 media and is echoed in international standards and policy frameworks. For instance, the United Nations  
91 System of Environmental-Economic Accounting advocates for vegetation as a nature-based approach to  
92 mitigate air pollution (Le Page et al., 2015). Vegetation primarily contributes to air pollution reduction through  
93 two mechanisms: deposition and dispersion (Shindell et al., 2012). Deposition involves the absorption of air  
94 pollutants onto vegetative surfaces, while dispersion refers to the reduction of air pollutant concentrations  
95 through aerodynamic effects caused by vegetation (Tiwari and Kumar, 2020; N. Wang et al., 2019a). Notably,  
96 Ramanathan et al. (2001) reported that dispersion effects are significantly more impactful than deposition,  
97 exceeding it by an order of magnitude via a radiative forcing modeling method.

99 However, the efficacy of dispersion effects resulting from UGS-LUCC in reducing air pollution is not  
100 straightforward. These effects can, under certain conditions, even increase local air pollution concentrations.  
101 These conditions are influenced by several factors, such as the specific structure of the UGS vegetation  
102 properties (e.g., height, leaf density), the site context (e.g., street canyon geometry, proximity to emission  
103 sources), and prevailing meteorological conditions (e.g., wind speed and direction) (~~Ramanathan et al., 2001;~~  
104 ~~Solomon, 2007);~~(Jin et al., 2017; Tomson et al., 2021; Yang et al., 2020). For example, dense tree canopies  
105 might impede ventilation in urban street canyons, while porous vegetation barriers in open-road settings could  
106 potentially intensify roadside air pollution concentrations (~~Allen and Ingram, 2002; Cohen et al., 2017);~~(Chen  
107 ~~et al., 2021; Jin et al., 2014).~~ Furthermore, ~~Seinfeld et al., (1998)~~Seinfeld et al., (1998) underscores the  
108 complexity of these interactions, and ~~they~~ demonstrated that vegetation could exert nonlinear effects on  
109 meteorological processes. These effects are particularly evident in their impact on the Planetary Boundary

110 Layer Height (PBLH) and the turbulent transport and advection of pollutants, which in turn influence  
111 dispersion conditions.

112  
113 UGS also have a complex role in air quality due to their production of biogenic volatile organic compounds  
114 (BVOCs). For instance, in cities like Los Angeles, the UGS-BVOC emissions contribute to a quarter of the  
115 secondary organic aerosol formation on hot days (Ramanathan et al., 2005). While Guenther et al., (2012)  
116 noted that the majority of BVOC emissions are from natural land cover, Ma et al., (2022) indicates that in  
117 metropolitan areas, the UGS-BVOC emissions can be significantly higher, ranging from 1 to 30 times those  
118 from natural land use cover. This evidence suggests a dual nature of UGS vegetation in urban environments:  
119 it can mitigate air pollution under certain conditions, but conversely, there is substantial experimental and  
120 modelling evidence showing it can exacerbate pollution under different circumstances (Allen and Ingram,  
121 2002; Burnett et al., 2018; Cohen et al., 2017). Moreover, metropolitan areas often encounter VOC limited  
122 conditions, or NO<sub>x</sub> saturation, where even minimal BVOC emissions can lead to notable O<sub>3</sub> production (Wang  
123 et al., 2019). Additionally, urban areas typically experience higher temperatures than their surrounding natural  
124 landscapes due to the urban heat island effect (Masson-Delmotte et al., 2021). This increase in temperature is  
125 likely to further amplify the UGS-BVOC emissions (Zhou et al., 2015), influencing O<sub>3</sub> concentrations  
126 significantly. This interaction might explain why many regional numerical models underestimate urban  
127 surface ozone levels, as they often lack high-resolution land use cover data necessary to accurately estimate  
128 the UGS-BVOC emissions (Qiu et al., 2023; Wang et al., 2021; Wu et al., 2020)(Schlaerth et al., 2023). While  
129 Guenther et al., (2012) noted that the majority of BVOC emissions are from natural land cover, Ma et al.,  
130 (2022) indicates that in metropolitan areas, the UGS-BVOC emissions can be significantly higher, ranging  
131 from 1 to 30 times those from natural land use cover. This evidence suggests a dual nature of UGS vegetation  
132 in urban environments: it can mitigate air pollution under certain conditions, but conversely, there is  
133 substantial experimental and modeling evidence showing it can exacerbate pollution under different  
134 circumstances (Allen and Ingram, 2002; Burnett et al., 2018; Cohen et al., 2017). Moreover, metropolitan  
135 areas often encounter VOC-limited conditions, or NO<sub>x</sub>-saturation, where even minimal BVOC emissions can  
136 lead to notable O<sub>3</sub> production (P. Wang et al., 2019). Additionally, urban areas typically experience higher  
137 temperatures than their surrounding natural landscapes due to the urban heat island effect (Masson-Delmotte  
138 et al., 2021). This increase in temperature is likely to further amplify the UGS-BVOC emissions (Zhou et al.,  
139 2015), influencing O<sub>3</sub> concentrations significantly. This interaction might explain why many regional  
140 numerical models underestimate urban surface ozone levels, as they often lack high-resolution land use cover

141 data necessary to accurately estimate the UGS-BVOC emissions (Qiu et al., 2023; Wang et al., 2021; Wu et  
142 al., 2020).

143  
144 ~~Currently, there is a growing research interest in characterizing the air quality impacts of UGS. While~~  
145 ~~Arghavani et al., (2019) investigating the effects of UGS on gaseous air pollutants in Tehran using the WRF-~~  
146 ~~Chem model, their focus was on the impact of meteorological changes on O<sub>3</sub> resulting from UGS (i.e., UGS-~~  
147 ~~LUCC effects), rather than the UGS-BVOC emissions effects on O<sub>3</sub>. In contrast, Schlaerth et al., (2023a)~~  
148 ~~addressed the influence of the UGS-BVOC emissions on O<sub>3</sub> in Los Angeles and their findings indicate that~~  
149 ~~the UGS-BVOC emissions may increase O<sub>3</sub> by 0.95 ppb during the daytime and decrease it by 0.41 ppb at~~  
150 ~~night. Despite Schlaerth et al., (2023a) illustrating the significance of the UGS-BVOC emissions on O<sub>3</sub>~~  
151 ~~concentrations, they did not investigate the impact of the UGS-LUCC effects.~~

152  
153  
154 Currently, there is a growing research interest in characterizing the air quality impacts of UGS. While  
155 Arghavani et al., (2019) investigated the effects of UGS on gaseous air pollutants in Tehran using the WRF-  
156 Chem model, their focus was on the impact of meteorological changes on O<sub>3</sub> resulting from UGS (i.e., UGS-  
157 LUCC effects), rather than the UGS-BVOC emissions effects on O<sub>3</sub>. In contrast, Schlaerth et al., (2023a)  
158 addressed the influence of the UGS-BVOC emissions on O<sub>3</sub> in Los Angeles and their findings indicate that  
159 the UGS-BVOC emissions may increase O<sub>3</sub> by 0.95 ppb during the daytime and decrease it by 0.41 ppb at  
160 night. Despite Schlaerth et al., (2023a) illustrating the significance of the UGS-BVOC emissions on O<sub>3</sub>  
161 concentrations, they did not investigate the impact of the UGS-LUCC effects.

162  
163 Surface O<sub>3</sub> is generally formed through chemical reactions of VOCs and NO<sub>x</sub> in the presence of sunlight. The  
164 nonlinear correlation between O<sub>3</sub> and concentrations of BVOC and NO<sub>x</sub> underscores the importance of  
165 examining potential interactions between the UGS-BVOC emissions and anthropogenic emissions.  
166 Furthermore, recent studies have highlighted the significance of the UGS-LUCC effects and the UGS-BVOC  
167 emissions effects. Given the rise in urban O<sub>3</sub> pollution, investigating the influence of the UGS-LUCC effects  
168 and the UGS-BVOC emissions effects on O<sub>3</sub> can assist in rationalizing UGS planning and formulating air  
169 quality mitigation strategies. However, there is a lack of quantification regarding the combined effects of  
170 UGS-LUCC and UGS-BVOC emissions on O<sub>3</sub>.

172 Situated in South China, Guangzhou is one of the rapidly expanding cities in China since the initiation of the  
173 reform and opening-up policy, undergoing swift urbanization (Yao and Huang, 2023). Being a key city in the  
174 Guangdong-Hongkong-Macao Greater Bay Area, Guangzhou places significant emphasis on UGS  
175 development. In this study, we aim to reconstruct the leaf area index (LAI) dataset for urban areas and estimate  
176 the UGS-BVOC emissions utilizing the Model of Emissions of Gases and Aerosols from Nature version 3.1  
177 (MEGANv3.1) (Guenther et al., 2020a). Subsequently, employing the Weather Research and Forecast model  
178 version 4.1.1 (WRFv4.1.1) (Salamanca et al., 2011) – Community Multiscale Air Quality model version 5.4  
179 (CMAQv5.4) (<https://zenodo.org/record/7218076>, last accessed: June 3, 2023), we intend to estimate the  
180 improvements of the CMAQ simulation performance from considering UGS-LUCC and UGS-BVOC and  
181 investigate the UGS-LUCC effects, the UGS-BVOC emissions effects, and their combined impacts on O<sub>3</sub> over  
182 Guangzhou by configuring sensitivity scenarios.

183 Situated in South China, Guangzhou (Figure 1) is one of the rapidly expanding cities in China since the  
184 initiation of the reform and opening-up policy, undergoing swift urbanization (Yao and Huang, 2023). Being  
185 a key city in the Guangdong-Hongkong-Macao Greater Bay Area, Guangzhou places significant emphasis on  
186 UGS development. In this study, we aim to reconstruct the leaf area index (LAI) dataset for urban areas and  
187 estimate the UGS-BVOC emissions utilizing the Model of Emissions of Gases and Aerosols from Nature  
188 version 3.1 (MEGANv3.1) (Guenther et al., 2020a). Subsequently, employing the Weather Research and  
189 Forecast model version 4.1.1 (WRFv4.1.1) (Salamanca et al., 2011) – Community Multiscale Air Quality  
190 model version 5.4 (CMAQv5.4) (<https://zenodo.org/record/7218076>, last accessed: June 3, 2023), we intend  
191 to estimate the improvements of the CMAQ simulation performance from considering UGS-LUCC and UGS-  
192 BVOC and investigate the UGS-LUCC effects, the UGS-BVOC emissions effects, and their combined  
193 impacts on O<sub>3</sub> over Guangzhou by configuring sensitivity cases.

## 194 2. Methods and data

### 195 2.1 Leaf area index and land cover dataset

196 The default LAI dataset to drive the MEGANv2.1 model which can used for MEGANv3.1 ~~model~~ is derived  
197 from the enhanced Moderate Resolution Imaging Spectroradiometer (MODIS) /MOD15A2H in 2003 with 1  
198 km spatial resolution (~~Myneni et al., 2015~~)(Myneni et al., 2015). As MODIS/MOD15A2H assigns an LAI  
199 value of 0 to urban areas, MEGANv3.1 compensates by averaging the LAI values in the vicinity of the urban

200 area. However, this approach introduces considerable uncertainty in the estimation of UGS-BVOC emissions.  
201 Hence, we opted for the Global Land Surface Satellite (GLASS) LAI product for MEGANv3.1 in 2017 with  
202 500-m spatial resolutions, derived from MODIS surface reflectance data using the bidirectional long short-  
203 term memory (Bi-LSTM) model, which leverages existing global LAI products (~~Ma and Liang, 2022~~)(Ma and  
204 [Liang, 2022](#)) and effectively incorporates the temporal and spectral information of MODIS surface reflectance.  
205 Consequently, the valid values of this data extend to urban areas, making it suitable for simulating the UGS-  
206 BVOC emissions.

207  
208 In this study, UGS are delineated as vegetation areas within the urban grid, and the urban grids are derived  
209 from MODIS/MCD12Q1 (~~Friedl and Sulla-Menashe, 2019~~) in 2017, which corresponds to the simulation  
210 ~~period with 500 m spatial resolution.~~(Friedl and Sulla-Menashe, 2019) in 2017, which corresponds to the  
211 [simulation period with 500 m spatial resolution](#). Furthermore, a high-resolution (10 m) land cover dataset in  
212 2017 was also obtained from the Geographic Remote Sensing Ecological Network Platform (accessible at  
213 <http://www.gisrs.cn/infofordata?id=1c089287-909e-4394-b07f-c7004be60884>, last accessed: 20/11/2023)  
214 and was employed to depict the spatial patterns of UGS. The processed land cover dataset is illustrated in  
215 Figure S1. Meanwhile, the use of high-resolution land use cover data is pivotal for accurately depicting the  
216 intricate details of land use cover, especially in areas broadly classified as urban by coarse-resolution data (i.e.,  
217 MCD12Q1) and this refined approach allows for a more precise differentiation of UGS. Specifically, we  
218 maintain a consistent urban area definition across both land use cover datasets, anchored by the urban  
219 delineation provided by the MCD12Q1 dataset. However, the coarse resolution of MCD12Q1 is insufficient  
220 for detailed spatial characterization of UGS. To address this limitation, we employ the high-resolution dataset  
221 to refine the characterization of non-urban surfaces within the urban boundaries (i.e., UGS) defined by  
222 MCD12Q1. This approach yields a sophisticated land cover dataset with 10 m spatial resolution that retains  
223 the urban extent delineated by MCD12Q1 while incorporating detailed representations of UGS absent in the  
224 original dataset. Consequently, while both datasets encompass identical urban extents, the default dataset lacks  
225 representations of UGS, in contrast to the high-resolution dataset, which includes detailed depictions of UGS.

## 226 2.2 MEGANv3.1 configuration

227 The calculation of BVOC emissions was performed utilizing MEGANv3.1 (accessible at  
228 <https://bai.ess.uci.edu/megan>, last accessed: 21 November 2023).~~MEGAN~~, which is a newly updated version.

MEGANv3.1 estimates BVOC emissions as the product of an emission factor and an emission activity factor (Guenther et al., 2012a, 2020a):

$$\text{Emission} = e \cdot \gamma \cdot \rho E = EF \times \gamma \quad (\text{Eq. 1})$$

In this equation,  $e$  ( $\text{mg} \cdot \text{m}^{-2} \cdot \text{h}^{-1}$ ) denotes an emission factor representing the emission rate under standard conditions;  $\rho$  signifies the production and consumption within the canopy, typically set as 1. In this equation,  $E$  is the net emission flux ( $\mu\text{g} \cdot \text{m}^{-2} \cdot \text{h}^{-1}$ ), and  $EF$  is the weighted average of the emission factor ( $\mu\text{g} \cdot \text{m}^{-2} \cdot \text{h}^{-1}$ ) for each vegetation type calculated by Emission Factor Processor (EFP). The emission activity factor ( $\gamma$ ) considers emission responses to changes in environmental and phenological conditions, and its calculation is as follows. Compare with earlier versions,  $\gamma$  in MEGANv3.1 adds quantifications for responses to high and low temperature, high wind speed, and air pollution ( $\text{O}_3$ ).

$$\gamma_i = C_{CE} \cdot \text{LAI} \cdot \gamma_{T,i} \cdot \gamma_{LA,i} \cdot \gamma_{SM,i} \cdot \gamma_{C,i} \cdot \gamma = \text{LAI} \times \gamma_{TP} \times \gamma_{LA} \times \gamma_{SM} \times \gamma_{HT} \times \gamma_{LT} \times \gamma_{HW} \times \gamma_{CO_2} \times \gamma_{BD} \times \gamma_{O_3} \quad (\text{Eq. 2})$$

In this equation, the activity factor for each compound class ( $i$ ) denotes the emission response to light ( $\gamma_P$ ), temperature ( $\gamma_T$ ), leaf age ( $\gamma_A$ ), soil moisture ( $\gamma_{SM}$ ), Leaf Area Index (LAI), and  $\text{CO}_2$  inhibition ( $\gamma_C$ ). The canopy environment coefficient ( $C_{CE}$ ) is assigned a value that ensures  $\gamma = 1$  under standard conditions and depends on the canopy environment model in use (Guenther et al., 2020a). In numerous applications of MEGAN, the activity factors for soil moisture and  $\text{CO}_2$  inhibition were disregarded (Guenther et al., 2012a; Sindelarova et al., 2014).

In this equation, the activity factor denotes the emission response to canopy temperature/light ( $\gamma_{TP}$ ), leaf age ( $\gamma_{LA}$ ), soil moisture ( $\gamma_{SM}$ ), high temperature ( $\gamma_{HT}$ ), low temperature ( $\gamma_{LT}$ ), high wind speed ( $\gamma_{HW}$ ), ambient  $\text{CO}_2$  concentration ( $\gamma_{CO_2}$ ), bidirectional exchange ( $\gamma_{BD}$ ),  $\text{O}_3$  exposure ( $\gamma_{O_3}$ ), and Leaf Area Index (LAI). In this study,  $\gamma_{CO_2}$  was not considered in the BVOC emission estimation. The MEGANv3.1 approach can calculate the emissions at each canopy level as the product of the emission factor and emission activity at each level.

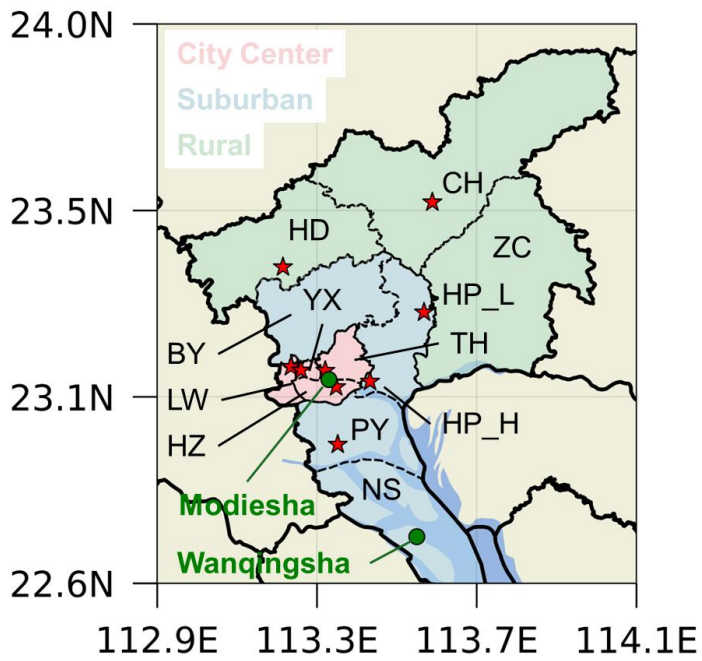
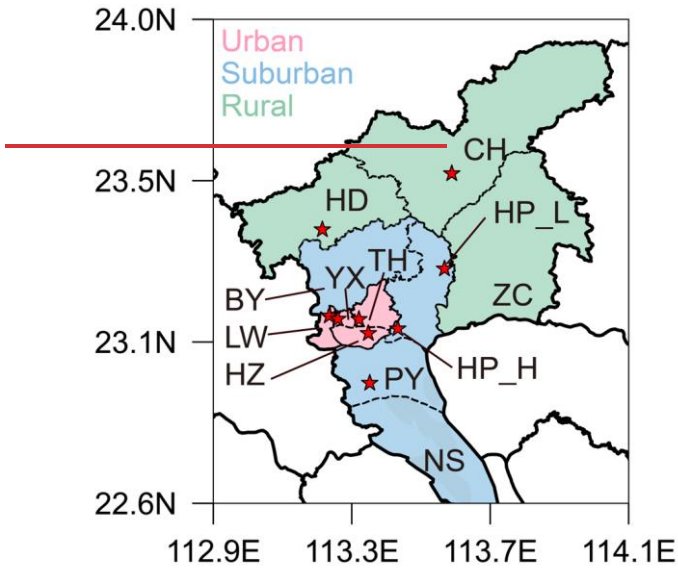
Hence, the input data to drive MEGANv3.1 comprises meteorological variables (e.g., temperature, solar radiation, relative humidity, soil moisture), LAI, and three types of land cover data (i.e., ecotype, growth

form, and relative vegetation composition for each ecotype/growth form). Meanwhile, the growth form datasets in MEGANv3.1 contain considerations of evergreen broadleaf forests, grasslands, and crops, which cover all types of UGS in Guangzhou city (Figure S1). Meteorological data are obtained from the WRF simulation results, and the LAI dataset is detailed in Section 2.1 as well as additional default land cover data provided by MEGANv3.1 were employed.

### 2.3 WRF-CMAQ and Scenario Case Configuration

Both the WRFv4.1.1 model and the CMAQv5.4 model are compiled and operated on a server with a Linux environment. The WRFv4.1.1 model was employed to simulate meteorological conditions, utilizing initial and boundary conditions sourced from the NCEP  $1^\circ \times 1^\circ$  Final (FNL) reanalysis dataset ([National Centers for Environmental Prediction, National Weather Service, NOAA, U.S. Department of Commerce, 2000](#))([National Centers for Environmental Prediction, National Weather Service, NOAA, U.S. Department of Commerce, 2000](#)). As illustrated in Figure S2, four nested domains with horizontal resolutions of 27, 9, 3, and 1 km, respectively, were employed. The outermost domain encompasses mainland China, while the innermost domain zooms in Guangzhou city, and the physical parameterization configured for the WRF simulation is listed in Table S1. CMAQv5.4 utilized meteorological fields provided by WRF to model  $\text{O}_3$  concentrations. The initial and boundary conditions for [the CMAQ model](#) were derived from the default profiles representing a clean atmosphere. In addition, we acquired anthropogenic emissions for the CMAQ domain from the Multi-resolution Emission Inventory for China (MEIC) 2017 developed by Tsinghua University, which contains monthly gridded ( $0.25^\circ \times 0.25^\circ$ ) emissions information for anthropogenic emissions. Moreover, [the CMAQ model](#) was configured with the Carbon Bond chemical mechanism (CB06) ([Luecken et al., 2019](#))([Luecken et al., 2019](#)) and AERO7 ([Pye et al., 2017](#))([Pye et al., 2017](#)). In this study, we incorporated the Modular Emission Inventory Allocation Tools for the Community Multiscale Air Quality model (MEIAT-CMAQ, <https://github.com/Airwhf/MEIAT-CMAQ>, last accessed: February 27, 2024) to allocate spatial and species-specific emissions within the raw inventories, addressing discrepancies in resolution and species compared to the modeled configurations. Moreover, MEIAT-CMAQ can directly generate the hourly model-ready emission files for CMAQ via temporal allocation. The model simulation spanned a month, from 21 August 2017 to 30 September 2017. To mitigate bias resulting from meteorological and chemical drift, the initial 10 days of this simulation were designated as spin-up and were not included in the analysis for this study. Given the spatial heterogeneity in the distribution of UGS across different areas, this study categorizes Guangzhou into

287 urbancity center, suburban, and rural regions (Figure 1). Specifically, the urbancity center areas comprise  
288 Haizhu (HZ), Liwan (LW), Yuexiu (YX), and Tianhe (TH) districts. The city center region has more UGS  
289 areas due to the higher urban land use and land cover fraction (Figure S1) compared to the suburban and rural  
290 regions. The suburban areas encompass Huangpu (HP), Baiyun (BY), Panyu (PY), and Nansha (NS) districts.  
291 Lastly, the rural regions include Zengcheng (ZC), Conghua (CH), and Huadu (HD) districts. To facilitate clear  
292 differentiation between the two sites in the HP region, they have been designated as HP\_L and HP\_H,  
293 respectively.



296 **Figure 1** The innermost domain of WRF-CMAQ with various areas and the air quality station locations map. Modiesha and Wangingsha  
297 are the observation sites for isoprene.  
298

299 In this study, four distinct scenarios/cases, as listed in Table 1, were established to investigate the impacts of  
300 UGS-LUCC, UGS-BVOC, and their combined effects on the ozone simulation. These scenarios/cases also  
301 focused on the performance of the CMAQ simulation and the influence on O<sub>3</sub> episodes. The Gdef\_N  
302 scenario/case considered as the base case, employs default land use cover data—specifically, data excluding  
303 UGS, and utilizes/uses the LAI dataset with urban areas omitted (N-LAI). In contrast, the Gdef\_Y scenario/case  
304 is similar to Gdef\_N but incorporates the LAI dataset that includes urban areas (T-LAI). This adjustment  
305 allows for the assessment of the UGS-BVOC emission effects on O<sub>3</sub> concentrations. The Ghr\_N scenario/case  
306 mirrors Gdef\_N but differs by integrating high-resolution land use cover data, which encompasses UGS land  
307 use cover. This scenario/case aims to examine the UGS-LUCC effects on O<sub>3</sub> concentrations. Finally, the Ghr\_Y  
308 scenario/case combines high-resolution land use cover data with the LAI dataset inclusive of urban areas,  
309 thereby enabling an exploration of the combined effects of UGS-BVOC emissions and UGS-LUCC on O<sub>3</sub>  
310 concentrations.

311  
312  
313  
314 **Table 1 ScenarioCase configurations**

Name	LC dataset	LAI dataset	Description
Gdef_N	Default data	N-LAI	Base
Gdef_Y	Default data	T-LAI	UGS-BVOC effects
Ghr_N	High-resolution data	N-LAI	UGS-LUCC effects
Ghr_Y	High-resolution data	T-LAI	combined effects

## 315 2.4 Observation Dataset

316 ~~We utilize hourly ground-level meteorological observations, encompassing 2-m temperature (T2) and 10-m~~  
317 ~~wind speed (WS10), sourced from national basic meteorological stations provided by the Guangdong~~  
318 ~~Provincial Meteorological Service (Figure S3). Hourly ambient concentrations of O<sub>3</sub> from national monitoring~~  
319 ~~stations are gathered from the China National Environmental Monitoring Centre (CNEMC). The locations of~~  
320 ~~these air quality stations are depicted in Figure 1, and the air quality data and meteorological data both undergo~~  
321 ~~thorough quality control. Subsequently, they are utilized to assess the model performance of WRF-CMAQ.~~

322 We use the hourly ground-level meteorological observations, encompassing 2-m temperature (T2) and 10-m

323 wind speed (WS10), sourced from national basic meteorological stations provided by the Guangdong  
324 Provincial Meteorological Service (Figure S3). Hourly ambient concentrations of O<sub>3</sub>, CO, and NO<sub>2</sub> from  
325 national monitoring stations are gathered from the China National Environmental Monitoring Centre  
326 (CNEMC; <http://www.cnemc.cn>, last assess: 24 December 4, 2024). The real-time hourly concentration of  
327 O<sub>3</sub> was measured by the ultraviolet absorption spectrometry method and differential optical absorption  
328 spectroscopy at each monitoring site. NO<sub>2</sub> concentrations are measured by the molybdenum converter method  
329 known to have positive interferences from NO<sub>2</sub> oxidation products (Dunlea et al., 2007).The instrumental  
330 operation, maintenance, data assurance, and quality control were properly conducted based on the most recent  
331 revisions of China Environmental Protection Standards (Zhang and Cao, 2015), and the locations of these air  
332 quality stations are depicted in Figure 1. Additionally, meteorological data also undergo thorough quality  
333 control. Subsequently, they are utilized to assess the model performance of WRF-CMAQ.

334  
335 For the isoprene (ISOP) evaluation, we use observation data from the Modiesha (23.11°N, 113.33°E) and  
336 Wanqingsha (22.71°N, 113.55°E) sites (Figure 1), where an online gas chromatography-mass  
337 spectrometry/flame ionization detector system (GC-FID/MSD, TH 300B, Wuhan) is used to measure VOCs  
338 in the ambient atmosphere. The system has a sampling rate of 60 mL/min for 5 minutes per sample, with a  
339 sampling frequency of once per hour (Meng et al., 2022). The ISOP observation data undergo rigorous quality  
340 control, which can be used for evaluating simulated ISOP concentrations. It is worth noting that the ISOP  
341 observational data for the Modiesha site covers September 2017, while the Wanqingsha site has data coverage  
342 from September 7 to September 30, 2017.

### 343 **3. Results and discussion**

#### 344 **3.1 Model Evaluation**

345 Evaluation of the WRF-CMAQ model performance is undertaken through comparison against ground-level  
346 observations and the evaluation metrics of meteorological parameters are listed in Table S2, which shows that  
347 the meteorological fields were faithfully reproduced in this study and can be used to drive the air quality model.

348  
349 The primary BVOCs are the major sources of isoprene (ISOP) and monoterpenes (monoterpene (TERP) are  
350 BVOCs), rendering the assessment of their concentrations a pivotal method for indirectly verifying the

accuracy of BVOC emission estimates. Table 2 delineated within this study presents the mean concentrations of ISOP and TERP derived from various scenarios cases juxtaposed with the observed average concentrations. This comparative analysis in the Modiesha site reveals that after the incorporation of the UGS-BVOC emissions, there is an augmentation in the ISOP concentration from 0.24 ppb to 0.31 ppb and from 0.24 ppb to 0.28 ppb under distinct land use cover scenarios cases (Gdef and Ghr), relative to an observed concentration of 0.33 ppb. Meanwhile, the evaluation at the Wanqingsha site, where the observed mean ISOP concentration was 0.45 ppb from September 7 to September 30, 2017, shows that the modeled ISOP concentrations increased from 0.29 to 0.31 ppb and from 0.27 to 0.29 ppb under distinct land use cover cases (Gdef and Ghr) when UGS-BVOC emissions were included. This increment signifies a substantial diminution in the discrepancy between the modeled and observed concentrations attributable to the UGS-BVOC emissions. Analogously, the integration of the UGS-BVOC emissions yields a refinement in the estimation accuracy of ISOP concentrations at both the Modiesha and Wanqingsha sites, as evidenced by a reduced bias.

These findings reveal that ISOP concentrations are underestimated by 26.19%, 36.36%, 16.4% and 34.7% in the Modiesha and Wanqingsha sites when UGS-BVOCs are excluded. Specifically, this range represents the proportion of ISOP originating from, respectively, suggesting the important role of UGS-BVOCs emissions in modeling. Moreover, numerous studies highlight the significant role of ISOP in ozone O<sub>3</sub> formation within the Pearl River Delta (PRD) region, including Guangzhou. For instance, Zheng et al., (2009) demonstrated that ISOP has the highest ozone formation potential among all VOCs. Therefore, incorporating UGS-BVOCs into ISOP concentration estimates is crucial for accurately modeling regional ozone O<sub>3</sub> levels.

**Table 2** Evaluation of the evaluation results for the monthly mean ISOP concentrations. The “Gdef\_N”, “Gdef\_Y”, “Ghr\_N”, and “Ghr\_Y” columns show the various metrics from comparing the hourly observation and simulation values during September 2017 for the Modiesha site and 7 September 2017 to 30 September 2017 for the Wanqingsha site.

Location	Observed	Observed	Reference			
Site name	Period	Concentration (ppb)	Gdef_N (ppb)	Gdef_Y (ppb)	Ghr_N (ppb)	Ghr_Y (ppb)

删除的单元格  
删除的单元格

Modies					0.28	Meng et al., (2022)
ha-	<del>20 Sep. 2017</del>					
(urban)	<del>20 Nov. 2017</del>	0.3329	0.2435	0.3123	0.2129	
23.11N,	2017Sim.					
113.33						
E						
	Obs.	0.34	0.34	0.34	0.34	
	MB	-0.06	0.01	-0.11	-0.05	
	NME	76.0%	68.7%	73.6%	66.2%	
	NMB	-16.4%	3.5%	-31.3%	-13.1%	
	R	0.44	0.46	0.37	0.39	
Wanqin			0.38			Meng et al., (2022)
sha-	<del>20 Sep. 2017</del>					
(suburb	<del>20 Nov. 2017</del>	0.4229	0.31	0.27	0.3529	
an)	2017Sim.					
22.43N,						
113.33						
E						
Wanqi						
ngsha						
	Obs.	0.45	0.45	0.45	0.45	
	MB	-0.15	-0.14	-0.17	-0.15	
	NME	58.9%	56.8%	60.4%	58.1%	
	NMB	-34.7%	-30.6%	-38.7%	-34.8%	
	R	0.35	0.39	0.34	0.4	

删除的单元格

删除的单元格

删除的单元格

379  
380 Additionally, various statistical metrics were ~~utilized~~used to assess the performance of hourly O<sub>3</sub>, MDA8 O<sub>3</sub>,  
381 and NO<sub>2</sub> and O<sub>3</sub> concentrations from the CMAQ simulation (~~Emery et al. 2017~~Emery et al. 2017). These  
382 metrics comprise the correlation coefficient (R), normalized mean bias (NMB), and normalized mean error  
383 (NME). The formulas for these metrics are listed in Table S3. ~~Emery et al. (2017) propose that the model~~  
384 ~~performs acceptably when NMB and NME of hourly O<sub>3</sub> concentrations are less than 15% and 25%,~~  
385 ~~respectively, and the correlation coefficient (R) is greater than 0.5. As illustrated in Table 3, it is evident that~~  
386 ~~all the scenarios exceed the specified requirement~~As shown in Table 3, the modeling performance for all cases  
387 are reasonably, albeit with some degree of underestimation. Despite these discrepancies, the model  
388 demonstrates sufficient reliability and can be effectively ~~utilized~~used in the subsequent research study.  
389 Meanwhile, the MBs of MDA8 O<sub>3</sub> across various cases indicate a substantial improvement in the CMAQ  
390 simulation when UGS-BVOC, UGS-LUCC, and their combined effects are considered. Specifically, the MB  
391 values decrease from -2.16 ppb in the Gdef N case to -0.26 ppb in the Ghr Y case, demonstrating that  
392 incorporating UGS-BVOC, UGS-LUCC, and their combined effects can enhance the accuracy of predicted  
393 daytime O<sub>3</sub> concentrations. In addition, we also evaluate the simulation performance for NO<sub>2</sub> in each

scenario case and the results suggest that all models have R above 0.63, and while there is some overestimation, the NMB is 15.0%, 15.2%, 13.0%, and 13.2% for Gdef\_N, Gdef\_Y, Ghr\_N, and Ghr\_Y, respectively. It should be emphasized that integrating UGS-BVOC into the modeling process can slightly improve the accuracy of NO<sub>2</sub> predictions, reducing the MB from 7.01 μg/m<sup>3</sup> 3.27 to 6.94 μg/m<sup>3</sup> 3.24 ppb, and from 6.09 μg/m<sup>3</sup> 2.84 to 6.03 μg/m<sup>3</sup> 2.81 ppb for Gdef and Ghr scenarios cases, respectively. The improvement in NO<sub>2</sub> predictions is attributed to the increased involvement of NO<sub>2</sub> in O<sub>3</sub> formation caused by the UGS-BVOC emissions, which reduces simulated NO<sub>2</sub> concentrations and narrows its bias against the observation.

**Table 3: The evaluation results for each scenario.**  
Evaluation results of the simulated monthly mean hourly O<sub>3</sub>, MDA8 O<sub>3</sub>, and hourly NO<sub>2</sub> mixing ratios for each case during September 2017.

Pollutant	Case name	Sim (μg/m <sup>3</sup> ppb)	Obs(μg/m <sup>3</sup> ppb)	MB(μg/m <sup>3</sup> ppb)	NMB	NME	R
Hourly O <sub>3</sub>	Gdef_N	60.4928.23	65.3330.49	-4.842.26	-6.7%	23.6%	0.82
	Gdef_Y	61.4328.67	65.3330.49	-3.901.82	-5.3%	23.6%	0.82
	Ghr_N	61.9128.89	65.3330.49	-3.421.60	-4.8%	22.5%	0.83
	Ghr_Y	62.8629.33	65.3330.49	-2.471.15	-3.4%	22.4%	0.83
MDA8 O <sub>3</sub>	Gdef_N	60.11	62.27	-2.16	-3.47%	21.71%	0.84
	Gdef_Y	61.04	62.27	-1.23	-1.97%	21.40%	0.84
	Ghr_N	61.07	62.27	-1.20	-1.92%	21.28%	0.84
	Ghr_Y	62.00	62.27	-0.26	-0.42%	21.23%	0.84
Hourly NO <sub>2</sub>	Gdef_N	53.0924.78	46.0721.50	7.013.27	15.2%	45.7%	0.63
	Gdef_Y	53.0224.74	46.0721.50	6.943.24	15.0%	45.5%	0.63
	Ghr_N	52.1724.35	46.0721.50	6.092.84	13.2%	43.8%	0.63
	Ghr_Y	52.1124.32	46.0721.50	6.032.81	13.0%	43.6%	0.63

In terms of O<sub>3</sub>, the UGS-BVOC, UGS-LUCC, and their combined effects have various performances in different regions (Table 4). These results indicate that the inclusion of UGS-BVOC emissions significantly remarkable influences MDA8 O<sub>3</sub> and hourly O<sub>3</sub> concentrations in urban region the city center region and this effect, primarily observed when comparing the Gdef\_Y with Gdef\_N and Ghr\_Y with Ghr\_N scenarios cases, is largely due to the VOC-limited areas prevalent in Guangzhou (He et al., 2024). (He et al., 2024). By integrating the UGS-BVOC emissions into the models (comparing Gdef\_Y and Gdef\_N scenarios cases), the bias MBs of MDA8 O<sub>3</sub> and hourly O<sub>3</sub> in all regions, including a notable improvement in the urban city center region from -7.77 μg/m<sup>3</sup> 3.62 to -0.75 ppb and -2.86 to -1.60 μg/m<sup>3</sup> 1.8 ppb, respectively, is reduced. Additionally, the UGS-BVOC emissions slightly enhance R values of MDA8 O<sub>3</sub> and hourly O<sub>3</sub> in the urban city center and suburban regions, indicating a more accurate MDA8 O<sub>3</sub> the daytime trend and the

diurnal cycle representation, respectively. The UGS-LUCC (land use and land cover change) effects, as seen when comparing Ghr\_N and Gdef\_N scenarios cases, also significantly greatly improve model biases and the combined effects of both UGS-BVOC and UGS-LUCC (comparing the Ghr\_Y and Gdef\_N scenarios cases) substantially ameliorate model biases in the urban city center and suburban regions.

**Table 4** The evaluation results of simulated monthly mean hourly O<sub>3</sub> and MDA8 O<sub>3</sub> mixing ratios in city center, suburban, and rural areas for O<sub>3</sub> in various regions each case during September 2017.

Variable Regions	Regions	MB ( $\mu\text{g}/\text{m}^3$ ppb)				R			
		Gdef_N	Gdef_Y	Ghr_N	Ghr_Y	Gdef_N	Gdef_Y	Ghr_N	Ghr_Y
Urban MD A8 O <sub>3</sub>	City center	-	-	-	-	0.805	0.810	0.810	0.813
		4.803	4.523	4.600	-0.747				
		3.627	2.241	2.110					
	Suburban	-	-	-	-	0.737	0.743	0.717	0.727
		8.737	6.967	6.880	5.093				
		4.076	3.251	3.210	2.376				
	Rural	-	-	-	-	0.665	0.655	0.695	0.690
		10.950	10.195	10.430	9.705				
		-5.109	-4.757	-4.866	4.528				
Hourly O <sub>3</sub>	City center	-2.862	-2.292	-2.086	-1.520	0.800	0.802	0.811	0.812
	Suburban	-3.148	-2.803	-2.647	-2.295	0.824	0.825	0.824	0.826
	Rural	-1.184	-1.630	-1.375	-1.164	0.742	0.741	0.751	0.750

插入的单元格

插入的单元格

插入的单元格

### 3.2 Estimation of UGS-BVOC emissions under different land use cover

This study comprehensively summarizes the UGS-BVOC emissions across various species for all regions in Guangzhou City in September. Given that the variances in the UGS-BVOC emissions due to different land use covers are relatively minor, the primary Table 5 presents emissions driven by the default land use cover. For a detailed breakdown of emissions attributable to varied land use covers, refer to Table S4. A review of the data reveals that monoethylene (TERP) and isoprene (ISOP) rank as the highest emitting species with proportions are 20.46% and 31.91% in this study, respectively, aligning with the findings of previous studies (Cao et al., 2022; Guenther et al., 2012b). Furthermore, Table 5 presents emissions driven by the default land use cover. For a detailed breakdown of emissions attributable to varied land use covers, refer to Table S4. A review of the data reveals that TERP and ISOP rank as the highest emitting species with proportions are 20.46% and 31.91% in this study, respectively, aligning with the findings of previous studies (Cao et al., 2022; Guenther et al., 2012b). Furthermore, Table 5 reveals that in September, the UGS-BVOC emissions in Guangzhou amounted to 666 Gg (~90 Mg/km<sup>2</sup>), with ISOP and TERP contributing remarkably to the total UGS-BVOC emissions. In comparison to anthropogenic VOC (AVOC) and BVOC emissions, UGS-BVOC emissions

account for approximately 33.45% in the city center region. Regionally, the suburban region registered the highest UGS-BVOC emissions in Guangzhou, peaking at 367.31 Gg. This is followed closely by the rural and urban city center regions, recording emissions of 173.65 Gg and 125.53 Gg, respectively.

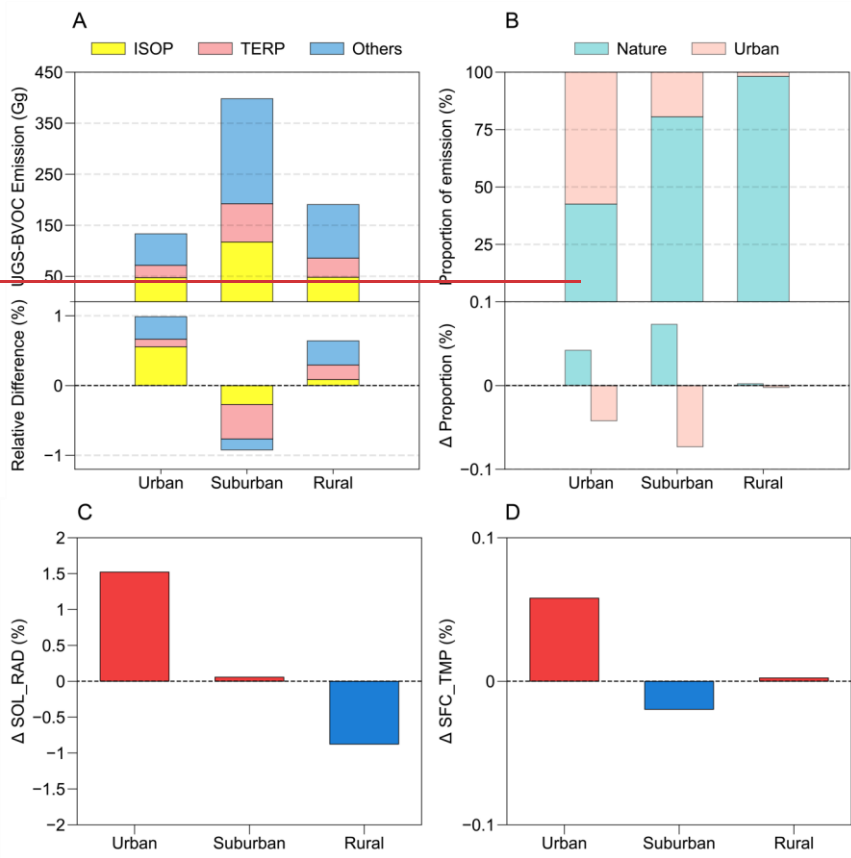
Table 5 The summarized table of UGS-BVOC emissions in Guangzhou city in September 2017 via default land use cover (units: Gg).

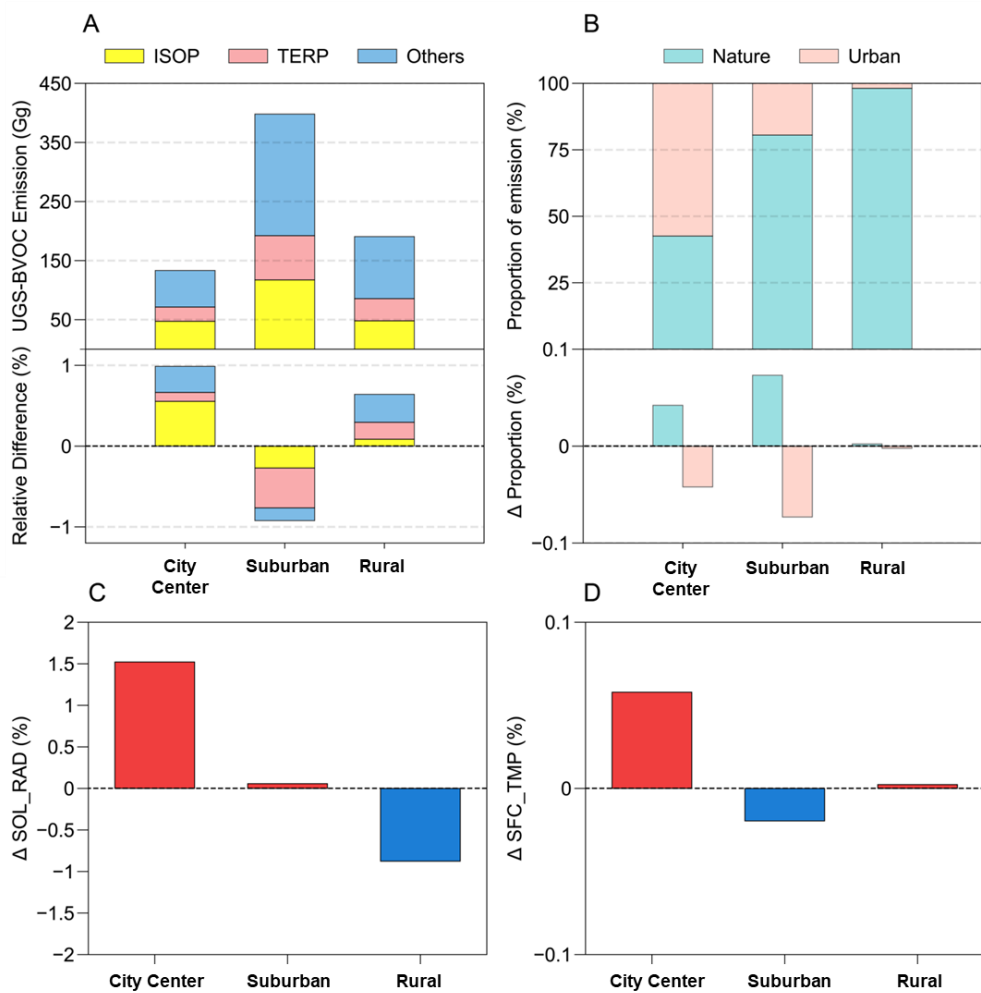
Species	Abbreviations	Urban City center (Gg)	Suburban (Gg)	Rural (Gg)	Total (Gg)
Acetic acid	AACD	0.86	2.44	1.18	4.48
Acetaldehyde	ALD2	3.46	11.57	5.83	20.86
Formaldehyde	FORM	0.95	3.90	2.17	7.02
Methanol	MEOH	12.47	41.31	20.36	74.14
Formic acid	FACD	2.79	7.84	3.79	14.42
Ethane	ETHA	2.12	8.40	4.64	15.16
Ethanol	ETOH	3.63	12.13	6.11	21.87
Acetone	ACET	6.22	21.52	11.63	39.37
Propane	PRPA	2.08	8.21	4.54	14.83
Ethene	ETH	3.97	15.64	8.64	28.25
Isoprene	ISOP	47.30	117.32	48.06	212.68
Monoterpenes	TERP	24.07	74.85	37.51	136.43
Alpha pinene	APIN	11.26	30.07	13.16	54.49
Methane	ECH4	0.04	0.14	0.08	0.26
Sesquiterpenes	SESQ	4.31	11.97	5.95	22.23
Total	Total	125.53	367.31	173.65	666.49

Figure 2-(A) provides a detailed illustration of the UGS-BVOC emissions across various regions in Guangzhou City, driven by default land use cover data, and compares these with the estimates derived from high-resolution land use cover data, which presents that the suburban region exhibits the highest UGS-BVOC emissions among the three studied regions, totaling 413.47 Gg. This predominance is linked to the larger extent of UGS in the suburban region, as depicted in Figure 5-(A), while the emissions in the urban city center and rural regions are reported at 137.69 Gg and 198.64 Gg, respectively. Moreover, UGS-LUCC is instrumental in modulating BVOC emissions, leading to an uptick in the urban city center and rural regions while precipitating a decline in the suburban region. Notably, a slight increase in solar radiation (SOL\_RAD) by 0.05% (Figure 2-(C)), attributable to a reduced urban fraction in the Ghr dataset, results in augmented solar exposure. Concurrently, a marginal reduction in surface temperature (SFC\_TMP) by 0.02% (Figure 2-(D)), facilitated by increased vegetation albedo cooling effects, underpins the decrease in UGS-BVOC emissions within suburban regions. This phenomenon underscores the critical role of lowered SFC\_TMP—driven by vegetation's higher albedo—in curtailing emissions stemming from UGS-LUCC. Moreover, in the urban city center contexts, the diminished urban fraction enhances SOL\_RAD and SFC\_TMP, promoting higher

457 emissions, a trend mirrored to a lesser extent in the rural region following the update of land use cover data to  
458 Ghr. Figure 2-(B) offers a clear depiction of the proportion of UGS-BVOC emissions relative to ~~natural/non-~~  
459 UGS area BVOC emissions in each region of Guangzhou City, which presents that the UGS-BVOC emissions  
460 in ~~urban regions~~the city center region constitute 57.34% of the total BVOC emissions in this region because  
461 of the larger urban proportions in the ~~urban~~city center region (Figure 5), while the UGS-BVOC emission  
462 proportion in suburban and rural are 19.44% and 1.86% respectively. This indicates a significant contribution  
463 of the UGS-BVOC emissions in the ~~urban~~the city center region. Furthermore, when examining the relative  
464 differences in the BVOC emissions resulting from various land use covers across the city, the changes are  
465 found to be minimal, which suggests that meteorological alterations from land use cover do not majorly  
466 influence the proportion of the UGS-BVOC emissions emanating in Guangzhou. Thus, factors other than land  
467 use changes might be more critical in shaping the distribution and intensity of the UGS-BVOC emissions in  
468 urban settings.

46p

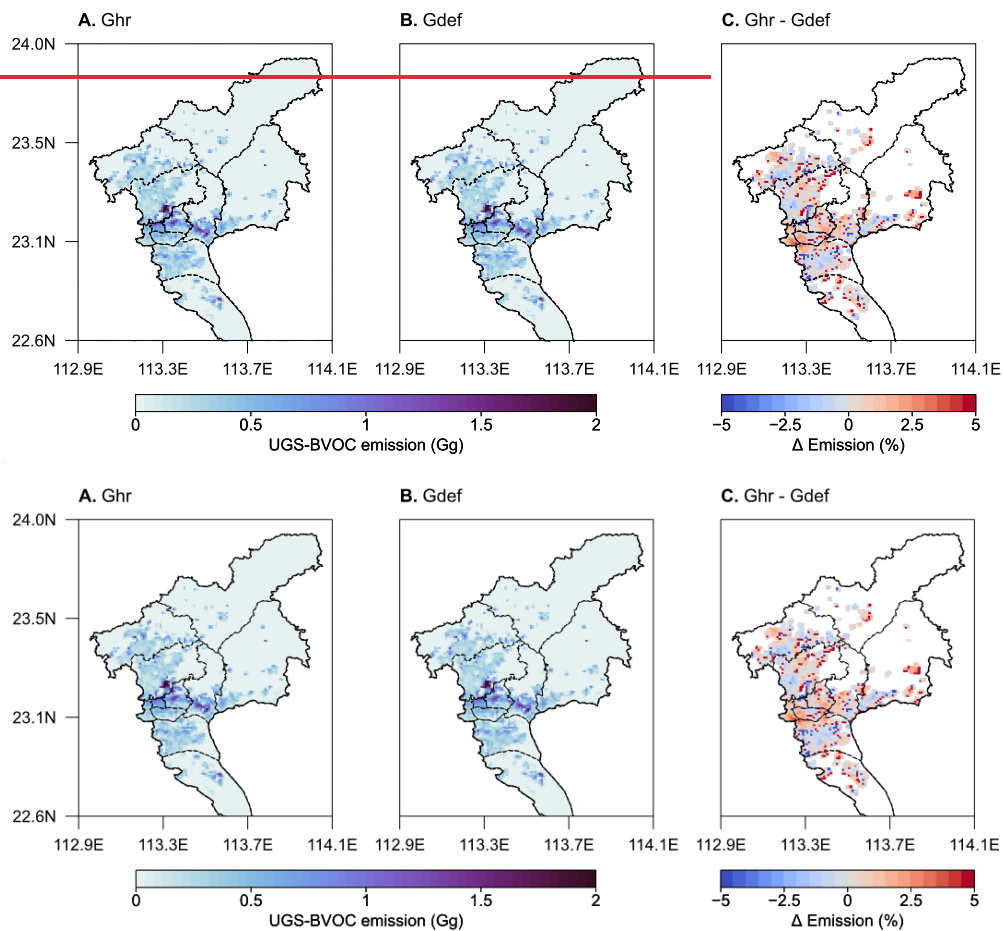




470  
471 **Figure 2** The UGS-BVOC emissions of each species and relative difference (Ghr - Gdef) from various land use cover (a), the proportion  
472 of emissions from urban and nature and the relative proportion difference (Ghr - Gdef) from various land use cover (b), the relative  
473 difference of solar radiation (C), and surface temperature (D) driven via various land use cover datasets. All values in these figure are  
474 during September 2017.  
475

476 Figure 3-(A) and (B) collectively highlight the patterns of the UGS-BVOC emissions across different land  
477 use covers, pinpointing the emission hotspots in urbancity center and suburban regions, which effectively  
478 illustrate how land use cover influences the UGS-BVOC emissions in various parts of the city. Additionally,  
479 Figure 3-(C) delves into the disparities in the UGS-BVOC emissions attributed to different land use cover  
480 datasets. It reveals that the variations in emissions are predominantly concentrated in the identified hotspots.

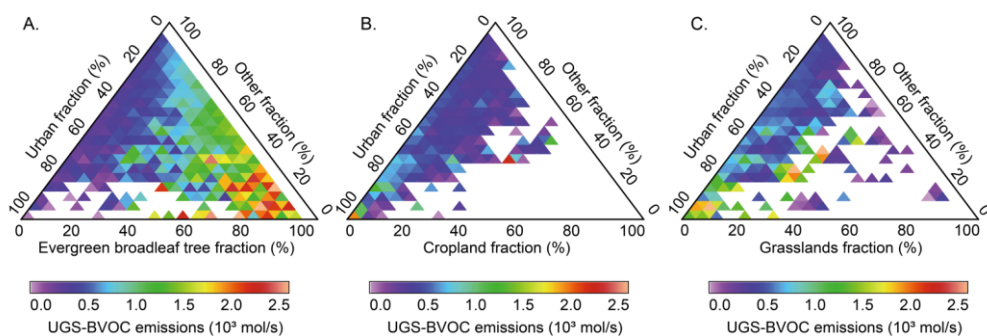
481 Moreover, Figure 3 (C) indicates that employing high-resolution land cover data typically results in marginally  
 482 higher estimates of the UGS-BVOC emissions, with an increase ranging between 0.8% to 2.9%. Figure 5-(E)  
 483 and (F) illustrate that despite a marginal reduction in solar radiation within ~~urban locales~~ the city center region,  
 484 a corresponding minor temperature elevation modestly boosts UGS-BVOC emissions, which presents that the  
 485 increase in temperature from UGS-LUCC causes the rise of the UGS-BVOC emissions.



487  
 488 **Figure 3** The UGS-BVOC emission maps in September 2017 from default (A) and high-resolution (B) land use cover, and the differences  
 489 of various UGS-BVOC emissions (C).

491 As illustrated in Figure S1, UGS in Guangzhou comprises three primary types of vegetation: evergreen  
 492 broadleaf forests, which are composed of Evergreen Broadleaf Trees (EBTs), cropland, and grasslands. This

493 classification has enabled a more nuanced understanding of how different types of UGS vegetation influence  
 494 UGS-BVOC emissions. Figure 4 reveals that EBTs predominate the urban vegetation landscape in Guangzhou  
 495 and are associated with higher rates of UGS-BVOC emissions as their coverage increases. Conversely, an  
 496 increase in the proportion of cropland correlates with reduced UGS-BVOC emissions, highlighting its minimal  
 497 contribution to the overall UGS-BVOC emissions of Guangzhou. Grasslands exhibit a variable impact on  
 498 BVOC emissions; when they constitute over 80% of the UGS, the emission rates are relatively low. However,  
 499 when grassland coverage ranges between 60-80%, its BVOC emissions surpass those from cropland within  
 500 the same percentage range. Overall, EBTs emerge as the primary contributors to UGS-BVOC emissions, with  
 501 grasslands and croplands making lesser contributions.

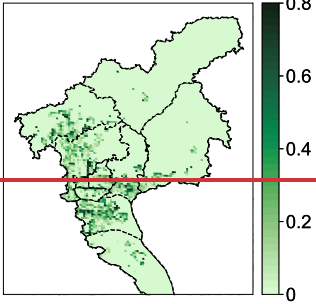


502 **Figure 4 Ternary heat map for various vegetation in UGS with the UGS-BVOC emission rate and the invalid value in this figure represents**  
 503 **no UGS-BVOC emission.**  
 504

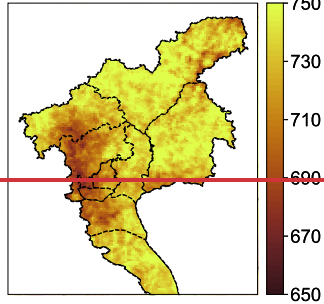
506 In addition to the proportion of UGS, the UGS-BVOC emissions in Guangzhou city are significantly  
 507 influenced by meteorological factors such as surface temperature and solar radiation (Guenther et al.,  
 508 2020b)(Guenther et al., 2020b). To elucidate the spatial heterogeneity of the UGS-BVOC emissions, this study  
 509 analyzes variations in these key factors. The simulation results depicted in Figure 5-(A) show the distribution  
 510 pattern of UGS, which are predominantly located in the urbancity center region, which account for a higher  
 511 percentage of the UGS-BVOC emissions compared to others. Interestingly, as indicated in Figure 5-(B), the  
 512 urbancity center region receives less solar radiation than other regions likely due to the shading effect of urban  
 513 canopies. Conversely, the urbancity center region exhibits elevated temperatures attributable to the urban heat  
 514 island effect, leading to an increase in UGS-BVOC emissions. Thus, while the distribution of UGS contributes  
 515 to the variation in the UGS-BVOC emissions across different regions, the more significant factor is the  
 516 enhanced UGS-BVOC emission due to higher temperatures in densely urbanized areas. The spatial dynamics

517 of the UGS-BVOC emissions are significantly shaped by two key meteorological factors: solar radiation and  
518 surface temperature. These elements independently play a crucial role in determining both the spatial pattern  
519 and the intensity of the UGS-BVOC emissions. Solar radiation directly influences the rate of photosynthesis  
520 and, consequently, the production of BVOCs, while temperature affects not only the physiological processes  
521 of vegetation but also the volatilization rate of these compounds (~~Fuhrer et al., 1997; Lombardozzi et al.,~~  
522 ~~2014~~);(Fuhrer et al., 1997; Lombardozzi et al., 2015). The intricate interplay between these factors leads to  
523 spatial variations in the UGS-BVOC emissions, with areas receiving higher solar radiation and experiencing  
524 warmer temperatures typically exhibiting more intense BVOC emissions.

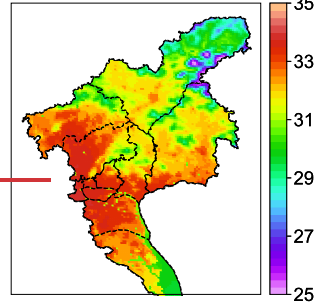
A. UGS fraction (%)



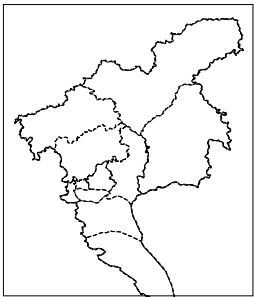
B. Solar radiation ( $W/m^2$ )



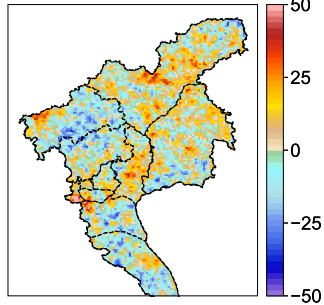
C. Temperature ( $^{\circ}C$ )



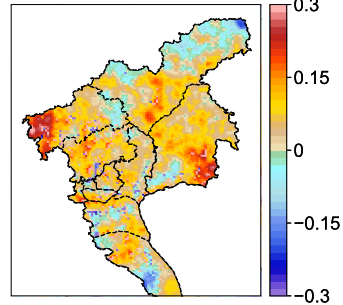
D. Significant LUCC grid



E.  $\Delta$  Solar radiation ( $W/m^2$ )



F.  $\Delta$  Temperature ( $^{\circ}C$ )



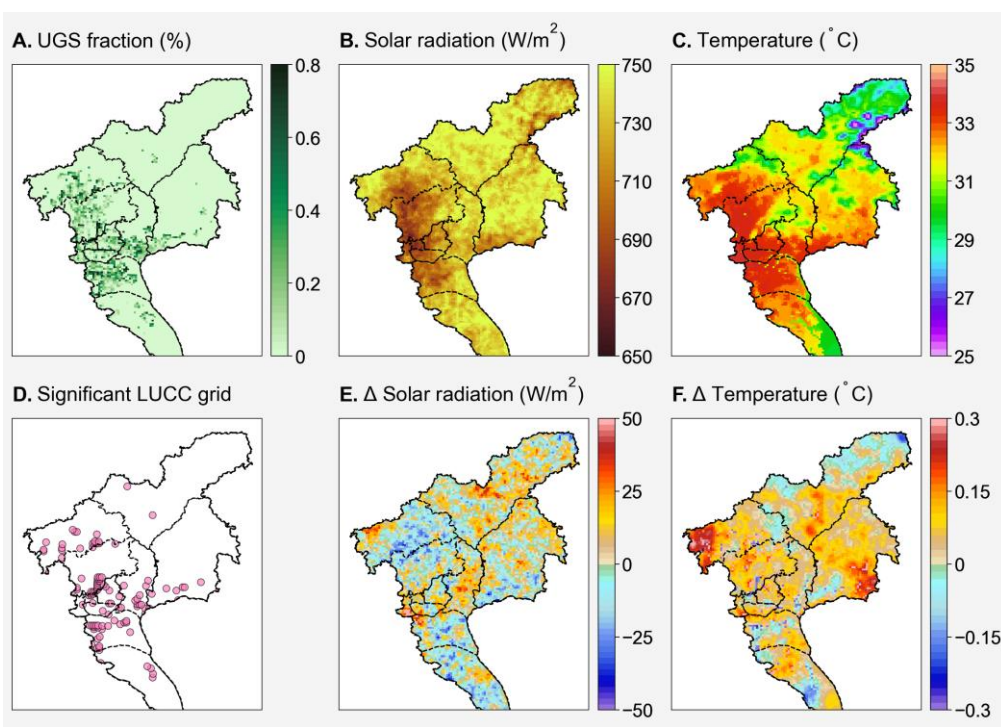


Figure 5 The UGS map (A) and the meteorological fields during September 2017 from the Ghr\_N scenario case (B and C). (D) is the grid locations where the land use experienced significant changes, (E) and (F) are the differences in solar radiation and temperature during the analysis periods (1 September 2017 to 30 September 2017) in various land use cover data (Ghr - Gdef).

This section has conclusively demonstrated that during the high O<sub>3</sub> season (September) in Guangzhou, the contribution of UGS-BVOC is substantial and cannot be overlooked and a notable finding is the strong spatial heterogeneity in these emissions across the city. The analysis also highlights high-resolution land use cover data increase the estimation of the UGS-BVOC emissions in the urban and suburban regions city center region.

### 3.3 Impact of UGS-LUCC and UGS-BVOC on Ozone Concentrations

The study evaluates the effects of UGS-BVOC and UGS-LUCC on MDA8 O<sub>3</sub> concentrations in Guangzhou, both individually and in combination. Figure 6 presents the absolute contributions from various cases, while the relative differences are shown in Figure S4. The analysis reveals that the UGS-BVOC emissions alone (Figure 6-A) primarily affect urban areas, significantly the city center region, greatly increasing MDA8 O<sub>3</sub> concentrations by 2.2-31.0 μg/m<sup>3</sup>-1.4 ppb (+2.3-3.2%), which increment aligns with findings from Los

Angeles, where ~~Schlaerth et al., (2023)~~ Schlaerth et al., (2023) reported a contribution of ~~1.2-5~~  $\mu\text{g}/\text{m}^3$  ppb from UGS-BVOC to urban MDA8 O<sub>3</sub> levels. N. Wang et al. (2019) reported that VOC levels can be highly sensitive in VOC-limited regions, where sufficient NO<sub>x</sub> concentrations mean that even a small disturbance in VOCs can cause significant changes in O<sub>3</sub> concentrations. Similarly, metropolitan areas, such as Guangzhou, often experience VOC-limited conditions or NO<sub>x</sub>-saturation (P. Wang et al., 2019). Consequently, the UGS-BVOC case results in an overall increase in MDA8 O<sub>3</sub>. In contrast, the sole impact of the UGS-LUCC effects (Figure 6-B) is more extensive, influencing both ~~urban~~ the city center and suburban regions and resulting in a general increase of approximately ~~1.1-2.3~~ ~~4.2~~  $\mu\text{g}/\text{m}^3$  ~~0~~ ppb (+2.3-4.3%) in MDA8 O<sub>3</sub> levels, which can be attributed to the higher temperature and solar radiation (Figure 5-(E)-(F)). In Guangzhou, the transformation of urban surfaces to natural vegetation due to UGS-LUCC results in lower albedo and consequently lower temperatures. However, this change also reduces the height of the urban canopy, diminishing its shading effects on solar radiation and paradoxically leading to higher temperatures in some regions. Therefore, considering the UGS-LUCC effect, the decreased urban canopy height could lead to elevated temperatures, thereby potentially increasing ozone production. However, the most significant results emerge under the combined effect of UGS-BVOC and UGS-LUCC (Figure 6-C), where a substantial increase in O<sub>3</sub> concentration, ranging from ~~1.7-3.6~~ ~~8.0~~  $\mu\text{g}/\text{m}^3$  ~~7~~ ppb (+3.8-8.5%), is observed across both ~~urban~~ the city center and suburban ~~areas~~ regions. The observed increase ~~highlights the critical~~ suggests a potentially significant influence of UGS-BVOC emissions and UGS-LUCC on ozone levels, ~~underlining the impossibility of overlooking~~ indicating that these factors ~~may play an important role~~ in ozone concentration ~~pollution~~ research, and should be carefully considered. This ~~revelation points to~~ finding underscores the essential role that integrated urban planning and environmental management play in controlling ozone pollution within metropolitan regions. By considering UGS-BVOC emissions in air quality models and management plans, managers can make more informed decisions to mitigate ozone levels and improve regional air quality.

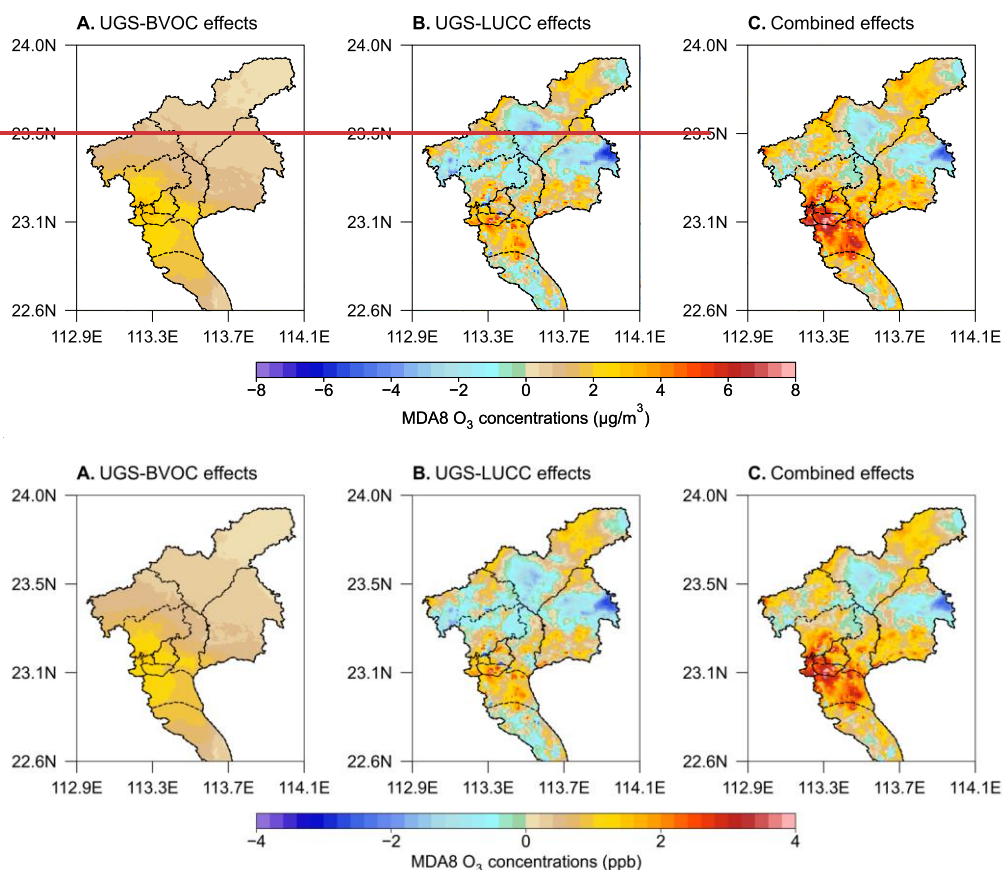
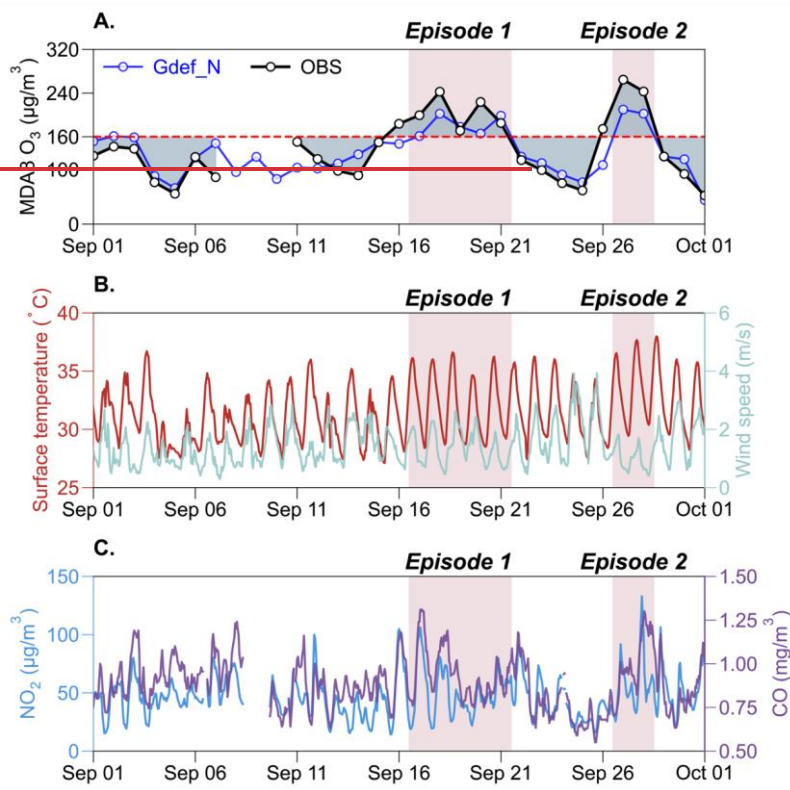


Figure 6 The map of UGS-BVOC effects (a), LUCC effects (b), and combined effects (c) in MDA8 O<sub>3</sub>. Each map shows the difference in average MDA8 O<sub>3</sub> concentrations for each case (Gdef\_Y, Ghr\_N, and Ghr\_Y) relative to the Gdef\_N case during September 2017.

Previous studies have established that O<sub>3</sub> episodes are often accompanied by high temperatures and intense solar radiation, conditions that can exacerbate the UGS-BVOC emissions, critically affecting air quality model performance (Shan et al., 2023; Soleimanian et al., 2023). (Shan et al., 2023; Soleimanian et al., 2023). In this study, an O<sub>3</sub> episode is defined as a period of two or more consecutive days with maximum daily average 8-hour (MDA8) O<sub>3</sub> concentrations exceeding 160 µg/m<sup>3</sup> (~80 ppb) (Wu et al., 2020). (Wu et al., 2020). Our analysis, as depicted in Figure 7(A), identified two such episodes in Guangzhou City during September: the first from September 16 to 21 and the second from September 26 to 28. The Gdef\_N scenario case successfully captures these episodes but tends to underestimate both MDA8 O<sub>3</sub> during these episodes. Figure 7(B) and (C) highlight a notable reduction in wind speed during both episodes, particularly during the second episode.

578 Despite some diffusion enhancement due to increased PBLH with rising surface temperatures (Figure S4S5),  
579 the surface temperature hike concurrently fosters O<sub>3</sub> production. Consequently, the episodes were dominated  
580 by a combination of temperature increases, which elevated O<sub>3</sub> concentrations, and wind speed decreases.  
581 Furthermore, Figure 7(C) illustrates that there was a significant spike in carbon monoxide (CO) concentrations  
582 during these episodes. CO, often used as a tracer in studies, indicates the worsening of diffusion conditions,  
583 leading to the accumulation of NO<sub>2</sub> - a primary O<sub>3</sub> precursor - thereby culminating in O<sub>3</sub> episodes in  
584 Guangzhou city.



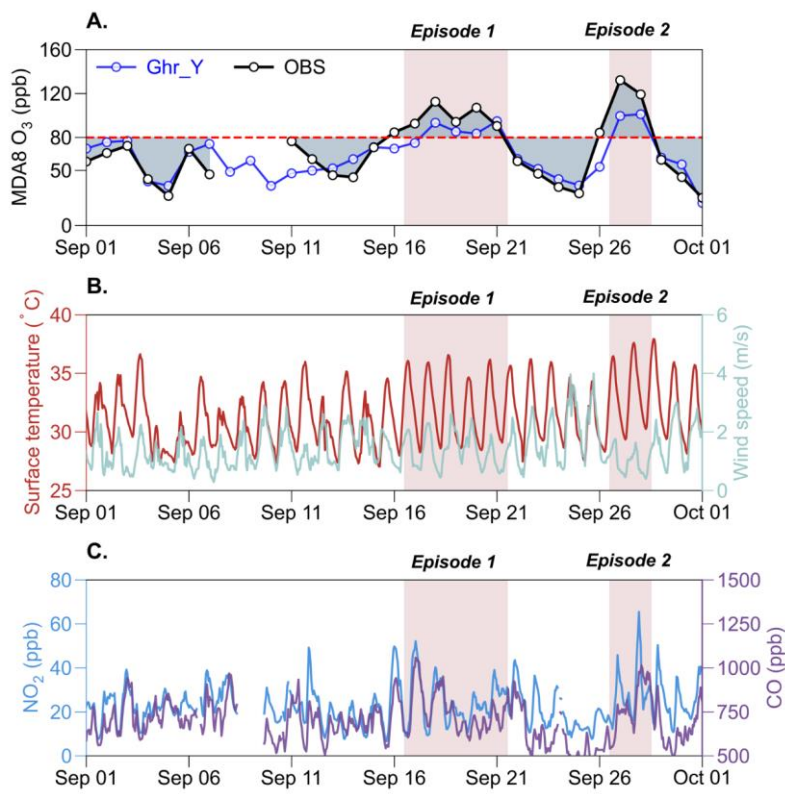


Figure 7 The comparison during September 2017 between the average values from simulation results grids which have air quality stations produced by the Gdef\_N scenario case and the average observation values for MDA8 O<sub>3</sub> (A). (B) are the meteorological fields from the average values from the simulation result grids, which have the same locations as the air quality stations. (C) are the observed average values for NO<sub>2</sub> and CO concentrations from all air quality stations.

Figure 8 presents that in assessing the simulation of O<sub>3</sub> episodes, the Gdef\_N scenario case, which initially underestimated O<sub>3</sub> concentrations, prompted an evaluation of improvements using different scenarios: UGS-LUCC (Ghr\_N), UGS-BVOC emissions (Gdef\_Y), and a combination of both (Ghr\_Y). The analysis, focusing on urban, the city-center, suburban, and rural stations, reveals that all scenarios tend to underestimate O<sub>3</sub> levels between both episodes. However, incorporating the UGS-BVOC emissions into the model results in a notable increase in mean simulated MDA8 O<sub>3</sub> concentrations, particularly in urban, the city center and suburban areas. For urban sites in the city center region, the mean simulated MDA8 O<sub>3</sub> increased by +3.21.6 and +6.3 μg/m<sup>3</sup> 2.9 ppb (+1.8% and +3.3%, respectively), while for suburban sites, the increase was +2.1.0 μg/m<sup>3</sup> 1.6 ppb (+1.1%) and +3.3 μg/m<sup>3</sup> 1.6 ppb (+1.9%), with rural sites experiencing a smaller

601 increase of only ~~+1.0~~  $\mu\text{g}/\text{m}^3$  0.5 ppb (+0.5%) and ~~+1.1~~  $\mu\text{g}/\text{m}^3$  0.5 ppb (+0.7%). This trend indicates a more  
602 pronounced impact in ~~urban~~ the city center and suburban ~~areas~~ regions compared to the rural region. Notably,  
603 the influence of the UGS-BVOC emissions on MDA8 O<sub>3</sub> in Episode 2 (~~+6.3~~  $\mu\text{g}/\text{m}^3$  2.9 ppb) was significantly  
604 greater than in Episode 1 (~~+3.2~~  $\mu\text{g}/\text{m}^3$  1.6 ppb), suggesting that meteorological conditions in Episode 2 were  
605 more conducive to the UGS-BVOC emissions, particularly in ~~urban areas~~ the city center region, which usually  
606 is VOC-limited areas.

607  
608 In Episode 1, the UGS-LUCC effects on O<sub>3</sub> concentrations were comparable to that of UGS-BVOC emissions,  
609 but in Episode 2, the UGS-LUCC effects led to a near doubling of urban MDA8 O<sub>3</sub> increase by ~~12.1~~  $\mu\text{g}/\text{m}^3$  5.9  
610 ppb (+6.48%) compared to the UGS-BVOC emissions. This indicates that the UGS-LUCC effects play a non-  
611 negligible role in O<sub>3</sub> pollution studies, and the response to such changes under different meteorological  
612 conditions varies significantly. Furthermore, due to the limited proportion of UGS in suburban and rural areas,  
613 the increased effect of UGS on O<sub>3</sub> is less pronounced in these regions, and nearly negligible in Episode 2.  
614 While the UGS-BVOC emissions alone have a modest effect on O<sub>3</sub> concentrations, their impact can become  
615 significant when combined with the UGS-LUCC effects. For instance, the combined effects in the ~~urban~~ city  
616 center region increased by ~~6.6~~  $\mu\text{g}/\text{m}^3$  3.2 ppb (+3.7%) and ~~18.7~~  $\mu\text{g}/\text{m}^3$  8.9 ppb (+10.0%) during Episode 1 and  
617 Episode 2, respectively.

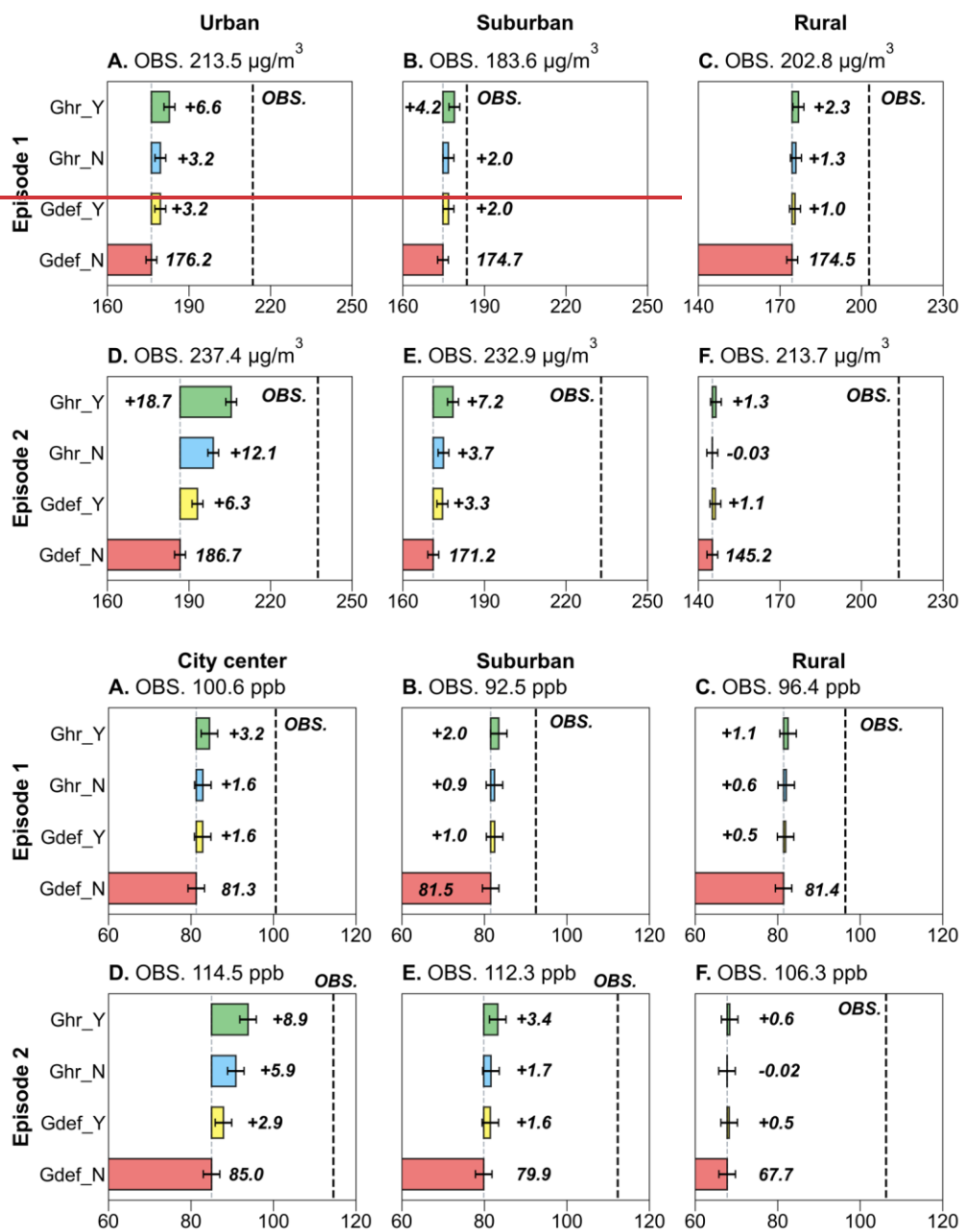
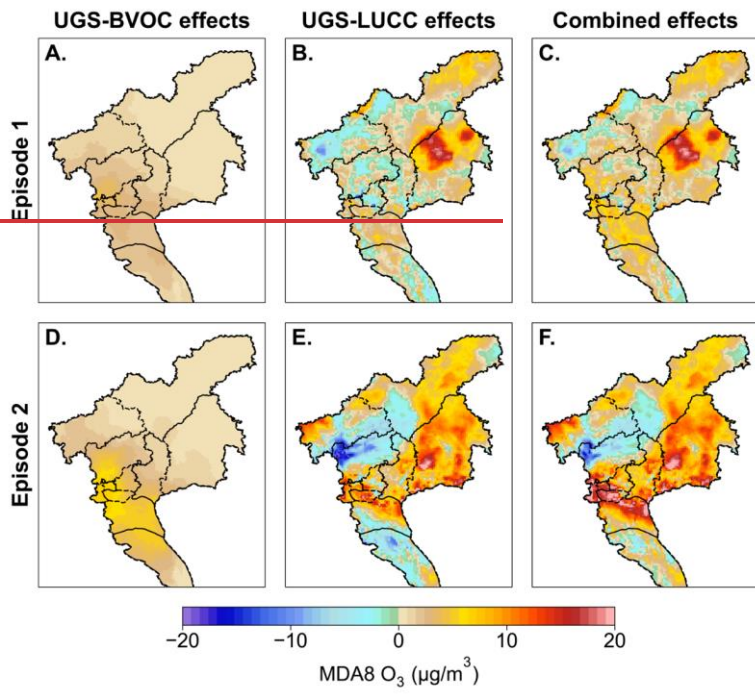
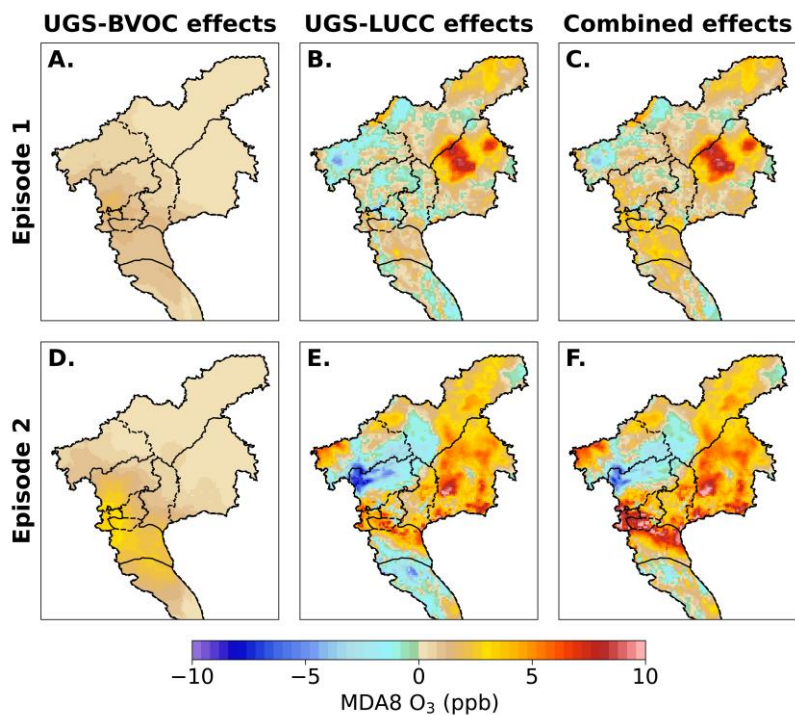


Figure 8 Comparison of simulated versus observed mean MDA8 O<sub>3</sub> concentrations across different scenarios/cases for two episodes. The figure is organized into columns representing urban (city center (4 sites), suburban (3 sites), and rural (2 sites) settings (columns 1-3,

622 respectively) and rows indicating comparisons for episode 1 and episode 2 (rows 1 and 2, respectively).

623  
624 Figure 9 presents the map of each effect on MDA8 O<sub>3</sub> in both episodes and the influence of UGS-BVOC  
625 emissions (Figure 9-(A) and (Figure 9D)) on the MDA8 O<sub>3</sub> concentration during Episode 1 and Episode 2  
626 ranges from 0 to ~~4.27~~ 4.27  $\mu\text{g}/\text{m}^3$  ~~2.0~~ 2.0 ppb and 0 to ~~7.43~~ 7.43  $\mu\text{g}/\text{m}^3$  ~~3.5~~ 3.5 ppb, respectively, with ~~urban areas~~ the city center  
627 region witnessing the most significant impact. This variance can be primarily ascribed to the heightened  
628 temperatures during Episode 2 (Figure 7-(B)), which create conditions more conducive to ozone generation  
629 through UGS-BVOC emissions. Furthermore, the UGS-LUCC effect's maximal contribution to the urban  
630 MDA8 O<sub>3</sub> levels could escalate to ~~4.62~~ 4.62  $\mu\text{g}/\text{m}^3$  ~~2.2~~ 2.2 ppb in Episode 1 and ~~50.90~~ 50.90  $\mu\text{g}/\text{m}^3$  ~~23.7~~ 23.7 ppb in Episode 2  
631 while the ~~eumulative~~ combined effects of UGS-LUCC and UGS-BVOC emissions are projected to enhance  
632 MDA8 O<sub>3</sub> concentrations to ~~10.31~~ 10.31  $\mu\text{g}/\text{m}^3$  ~~4.8~~ 4.8 ppb and ~~53.93~~ 53.93  $\mu\text{g}/\text{m}^3$  ~~25.2~~ 25.2 ppb for the respective episodes. This  
633 marked increase in the episodes' contributions can be linked to the differential responsiveness of land use data  
634 under various meteorological conditions. Notably, while the contribution from the UGS-BVOC effect during  
635 Episode 2 substantially exceeds that of Episode 1, the incremental impact of UGS-LUCC on combined effects  
636 in Episode 2 is notably smaller than in Episode 1. This phenomenon indicates that the escalated UGS-BVOC  
637 emissions in Episode 2 may start to inhibit ozone production rates incrementally.

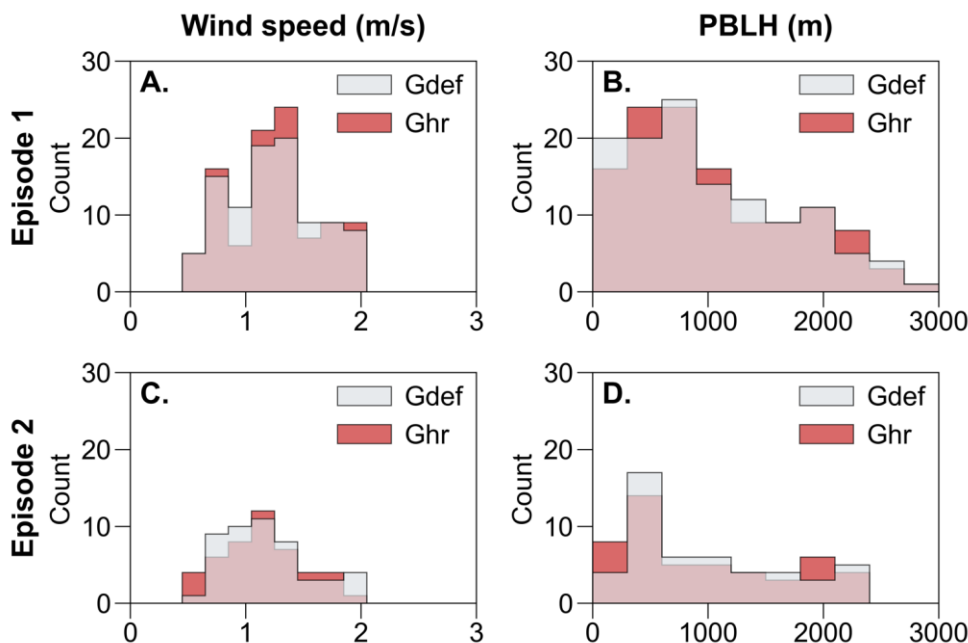




639  
640 Figure 9 The UGS-BVOC effects (A, D), the UGS-LUCC effects (B, E), and the combined effects (C, F) in Episode 1 and Episode 2,  
641 respectively.

642  
643 Figure 8 reveals that both observed O<sub>3</sub> episodes were primarily caused by reduced diffusion conditions.  
644 Notably, the impact of the UGS-LUCC effects varied significantly between the two episodes. Analysis of  
645 meteorological variables, specifically wind speed and PBLH, which are crucial for diffusion, demonstrate  
646 distinct patterns. Figure 10 illustrates that during Episode 1, the UGS-LUCC effects led to a notable increase  
647 in the frequency of higher wind speeds at (1.2–1.4 m/s, while simultaneously reducing) and a simultaneous  
648 decrease in the frequency at of lower wind speeds (0.9–1.1 m/s, which indicates). This shift in the wind speed  
649 distribution suggests an overall increase in average wind speed due to the UGS-LUCC effects during Episode  
650 1. In contrast, Episode 2 experiences a significant decrease in wind speed frequency at 0.7-1.1 m/s, with an  
651 increase in the lower range of 0.5-0.7 m/s. This suggests that the UGS-LUCC effects further reduce the already  
652 low wind speeds in Episode 2. Concerning PBLH, the UGS-LUCC effects are observed to elevate PBLH  
653 during Episode 1, which led to a decrease in PBLH during Episode 2. Therefore, the UGS-LUCC effects are  
654 markedly more pronounced in Episode 2 than in Episode 1, contributing to a more substantial alteration of

655 meteorological conditions affecting air dispersion and, consequently, O<sub>3</sub> formation.



656  
657 **Figure 10** The frequency of wind speed (column 1) and PBLH (column 2) in Episode 1 (row 1) and Episode 2 (row 2) driven by different  
658 land use cover datasets.

659 4  
660 错误!未找到引用源。 presents the overall results for the impacts of UGS-LUCC and UGS-BVOC on MDA8  
661 O<sub>3</sub> concentrations. The effects show slight variations across different regions during September, while the  
662 effects during the two episodes exhibit more significant changes. In the city center region, which shows the  
663 largest changes, the UGS-BVOC effect shows increases by +1.6 ppb in Episode 1 and +5.9 ppb in Episode 2,  
664 indicating that the UGS-BVOC effects influence MDA8 O<sub>3</sub> concentrations in the city center during ozone  
665 episodes, while their impact is minimal in suburban and rural regions. These results highlight the important  
666 effects of UGS-LUCC and UGS-BVOC in urban areas, especially during O<sub>3</sub> pollution periods.

667 **Table 6** Summary of Average MDA8 O<sub>3</sub> Concentrations (ppb) for Various Effects during September 2017.

Regions	Periods	UGS-BVOC effect	UGS-LUCC effect	Combined effect
City center	Monthly	+0.4	0.0	0.4
	Episode 1	+1.6	+1.6	+3.2
	Episode 2	+2.9	+5.9	+8.9
Suburban	Monthly	+0.4	0.0	0.4
	Episode 1	+1.5	+0.9	+2.0
	Episode 2	+1.6	+1.7	+3.4

	<u>Monthly</u>	<u>+0.4</u>	<u>0.0</u>	<u>0.4</u>
<u>Rural</u>	<u>Episode 1</u>	<u>+0.5</u>	<u>+0.6</u>	<u>+1.1</u>
	<u>Episode 2</u>	<u>+0.5</u>	<u>0.0</u>	<u>+0.5</u>

#### **4. Uncertainties and Limitations**

In this study, we used land use and land cover data integrated at 1-km and 10-m resolutions to define the urban boundary and characterize the spatial distribution of UGS in Guangzhou. Additionally, we incorporate high-resolution LAI data, obtained through machine learning, as input for the MEGAN model. Using the WRF-CMAQ model, we quantify the effects of UGS-BVOC, UGS-LUCC, and their combined impacts on ozone concentrations in Guangzhou. However, some uncertainties and limitations remain.

First, the 10-m resolution land use and land cover data still cannot fully capture the spatial pattern of UGS in Guangzhou. As shown in Figure S2, although UGS in Guangzhou is primarily composed of EBTs, most of these EBTs are distributed along urban edges. This may result from distortions in the definition of urban extent, such as misclassifying mixed urban-vegetation grids as urban grids, caused by the coarse resolution of the 1-km land use and land cover data. The fuzzy definition of urban boundaries could lead to non-UGS areas being misclassified as UGS, potentially resulting in an overestimation of UGS-BVOC emissions.

Second, due to resolution limitations, only larger patches of grassland, cropland, and woodland are recognized as UGS, while smaller UGS vegetation, such as street trees, often goes undetected at a 10-m resolution. This omission can lead to an underestimation of the UGS-BVOC emissions.

Third, the 10-m and 1-km resolution land use and land cover data, along with the growth forms and ecotype data, use simplified categorizations for grids, which cannot fully capture the diversity of vegetation species within UGS. Since different vegetation species have varying emission factors, this simplification introduces some errors. Similarly, the oversimplified classification of land grids limits this study's ability to provide specific planning strategies for UGS at the species level. Nevertheless, it can highlight the importance of considering UGS-BVOC and UGS-LUCC in air pollution prevention and control policies.

Finally, Guangzhou, the study area, is a highly urbanized Chinese metropolis with a VOC-limited region

(Gong et al., 2018; Kai et al., 2011; Liu et al., 2021). As a result, even a relatively small amount of VOC emissions, such as those from UGS-BVOC, can significantly impact ozone concentrations. Therefore, policymakers in Guangzhou should prioritize addressing the role of UGS-BVOC emissions in air pollution prevention and control. In other cities, particularly those with advanced urban development, high NO<sub>x</sub> emissions—often resulting from factors like high motor vehicle ownership—can lead to VOC-limited conditions. In such areas, it is equally important to emphasize the role of UGS-BVOC emissions in ozone pollution. In contrast, cities with lower NO<sub>x</sub> emissions identified as NO<sub>x</sub>-limited regions may experience minimal impact from UGS-BVOC emissions on ozone concentrations.

## 5. Conclusion

The rapid urbanization process ~~was~~ accompanied by a higher frequency of ozone episodes. It has been increasingly recognized that UGS can potentially exacerbate ozone pollution under specific conditions due to the UGS-LUCC and UGS-BVOC emissions. Guangzhou, located in ~~the South of southern~~ China, and known as a pioneer city in reform and opening-up policies, has experienced rapid urbanization over the past thirty years, ~~accompanied by the challenge of leading to increased challenges with~~ ozone pollution. Despite efforts to reduce anthropogenic emissions, ozone episodes occur with relatively high frequency in Guangzhou. This study selected September 2017, a month with a high incidence of ozone episodes in Guangzhou, to estimate the UGS-BVOC emissions using the WRF-MEGAN model and quantitatively assess the impact of UGS-LUCC, UGS-BVOC, and their combined effects on two ozone episodes in September 2017 using the CMAQ model. The major findings are shown as follows.

1. In September 2017, the UGS-BVOC emissions in Guangzhou totaled 666.49 Gg, with ISOP and TERP as the ~~primary~~major species, emitting 212.68213 and 136.43 Gg, respectively. Spatially, UGS-BVOC emissions were predominantly located in ~~urban areas~~the city center region, attributed to the more extensive distribution of UGS there. The study also indicates that meteorological changes caused by UGS-LUCC do not significantly affect UGS-BVOC emissions. Instead, the formation of emission spatial distribution and intensity is closely related to local surface temperature and solar radiation. This understanding underscores the importance of considering local solar radiation and temperature conditions when assessing and modeling the distribution of the UGS-BVOC emissions, as they are

pivotal in driving the spatial characteristics of these emissions. ~~Moreover, EBTs, which are the main vegetation type in the UGS of Guangzhou and a significant source of UGS BVOCs, provide a reference for future urban greening in the city to select species with lower emission factors as the primary vegetation types.~~

2. Considering ~~the~~ UGS-BVOC and UGS-LUCC ~~effects~~ can effectively mitigate the underestimation of surface ozone concentrations by regional air quality models, ~~though other factors such as inaccuracies in emissions inventories, chemical mechanisms, and meteorological inputs may also contribute to these underestimations.~~ For instance, incorporating UGS-BVOC emissions results in an increase in ISOP concentration from 0.2429 ppb to 0.3135 ppb and from 0.2423 ppb to 0.2829 ppb under different land use ~~scenarios~~ (Gdef and Ghr), compared to a baseline concentration of 0.3335 ppb. This significant enhancement in ISOP concentrations—the predominant component in BVOCs and the most crucial VOC for O<sub>3</sub> formation in the PRD—highlights two key points. Firstly, it indicates an improvement in the accuracy of BVOC concentration simulations. Secondly, this precise estimation of BVOCs has notably shifted the MB of O<sub>3</sub> simulations from 7.77 μg/m<sup>3</sup>3.62 ppb to -1.60 μg/m<sup>3</sup>0.75 ppb in ~~urban areas~~the city center region. Additionally, the simulation of NO<sub>2</sub> concentrations also shows slight improvements, with the MB decreasing from 7.01 μg/m<sup>3</sup>3.27 ppb to 6.03 μg/m<sup>3</sup>2.81 ppb upon accounting for UGS-BVOCs and UGS-LUCC. Given that the UGS are often located in densely populated urban regions, their inclusion in air quality simulations is crucial for accurately modeling urban air quality.
3. The UGS-BVOC emissions have a ~~significant~~remarkable impact on ozone concentrations, with increases ranging from 1.0-1.4 ppb (+2.3-3.2-3.0 μg/m<sup>3</sup>%) in ~~urban~~the city center regions. However, when considering the combined UGS-LUCC and UGS-BVOC effects, the impact on MDA8 O<sub>3</sub> concentrations becomes ~~significant~~remarkable, with values ranging from 1.7-3.6-7 ppb (+3.8-0 μg/m<sup>3</sup>-8.5%) in ~~urban regions~~the city center region. This indicates the importance of considering both UGS-LUCC and UGS-BVOC impacts when discussing the influence of UGS on air quality. Since UGS exhibits different effects in various ozone episodes, it is found that the impact of UGS on ozone levels is related to specific meteorological conditions. In the episodes of this study, the combined effects on MDA8 O<sub>3</sub> can reach up to 18.7 μg/m<sup>3</sup>8.9 ppb in ~~urban regions~~the city center region.

This study on ozone pollution in Guangzhou provides key insights for other cities on integrating UGS with air quality management. By including UGS-BVOC emissions and UGS-LUCC in the air quality model, the

755 study demonstrates improved accuracy in predicting surface ozone concentrations, which can aid urban  
756 planners and environmental policymakers in refining their strategies to better address urban air pollution.  
757 Moreover, these findings encourage cities to integrate urban forestry into their land use planning and air quality  
758 frameworks, promoting environmental sustainability amid rapid urbanization.

### 759 **Data availability**

760 The WRF (Weather Research and Forecasting Model) code can be obtained from the official repository at  
761 <https://github.com/wrf-model/WRF>. The CMAQ (Community Multiscale Air Quality Model) code is  
762 accessible at <https://github.com/USEPA/CMAQ>. Model output data used for analysis and plotting, and the  
763 code used for simulations can be made available upon request (Haofan Wang, [wanghf58@mail2.sysu.edu.cn](mailto:wanghf58@mail2.sysu.edu.cn)).

### 764 **Author contributions**

765 HFW conceived the study, carried out the model simulations, and drafted the manuscript. ~~YJL and THZ~~  
766 completed the data visualization. YML conceived and supervised this study, and reviewed and edited the paper.  
767 XL and YZ provided useful comments on the paper. QF supervised and funded the study. CS provided the  
768 meteorological data for model evaluation. SCL, YZ, TZ, and DLY provided the observation data for the  
769 evaluation of isoprene simulation.

### 770 **Competing interests**

771 The contact author has declared that neither they nor their co-authors have any competing interests.

### 772 **Acknowledgment**

773 The authors would like to thank the MEIC team from Tsinghua University for providing the anthropogenic  
774 emissions for this study. Meanwhile, we also thank Tianhe-2 for providing the computer resources.

## Financial support

This work is jointly funded by the innovation Group Project of Southern Marine Science and Engineering Guangdong Laboratory (Zhuhai) (316323005), Guangdong Basic and Applied Basic Research Foundation (2020B0301030004, 2023A1515110103, 2023A1515010162), National Natural Science Foundation of China (42105097, 42075181, 42375182), Guangdong Science and Technology Planning Project (2019B121201002), and Science and Technology Planning Project of Guangzhou (2023A04J1544).

## Reference

- Allen, M.R., Ingram, W.J., 2002. Constraints on future changes in climate and the hydrologic cycle. *Nature* 419, 224–232. <https://doi.org/10.1038/nature01092>
- Arghavani, S., Malakooti, H., Bidokhti, A.A., 2019. Numerical evaluation of urban green space scenarios effects on gaseous air pollutants in Tehran Metropolis based on WRF-Chem model. *Atmos. Environ.* 214, 116832. <https://doi.org/10.1016/j.atmosenv.2019.116832>
- Burnett, R., Chen, H., Szyszkowicz, M., Fann, N., Hubbell, B., Pope, C.A., Apte, J.S., Brauer, M., Cohen, A., Weichenthal, S., Coggins, J., Di, Q., Brunekreef, B., Frostad, J., Lim, S.S., Kan, H., Walker, K.D., Thurston, G.D., Hayes, R.B., Lim, C.C., Turner, M.C., Jerrett, M., Krewski, D., Gapstur, S.M., Diver, W.R., Ostro, B., Goldberg, D., Crouse, D.L., Martin, R.V., Peters, P., Pinault, L., Tjepkema, M., van Donkelaar, A., Villeneuve, P.J., Miller, A.B., Yin, P., Zhou, M., Wang, L., Janssen, N.A.H., Marra, M., Atkinson, R.W., Tsang, H., Quoc Thach, T., Cannon, J.B., Allen, R.T., Hart, J.E., Laden, F., Cesaroni, G., Forastiere, F., Weinmayr, G., Jaensch, A., Nagel, G., Concin, H., Spadaro, J.V., Burnett, R., Chen, H., Szyszkowicz, M., Fann, N., Hubbell, B., Pope, C.A., Apte, J.S., Brauer, M., Cohen, A., Weichenthal, S., Coggins, J., Di, Q., Brunekreef, B., Frostad, J., Lim, S.S., Kan, H., Walker, K.D., Thurston, G.D., Hayes, R.B., Lim, C.C., Turner, M.C., Jerrett, M., Krewski, D., Gapstur, S.M., Diver, W.R., Ostro, B., Goldberg, D., Crouse, D.L., Martin, R.V., Peters, P., Pinault, L., Tjepkema, M., van Donkelaar, A., Villeneuve, P.J., Miller, A.B., Yin, P., Zhou, M., Wang, L., Janssen, N.A.H., Marra, M., Atkinson, R.W., Tsang, H., Quoc Thach, T., Cannon, J.B., Allen, R.T., Hart, J.E., Laden, F., Cesaroni, G., Forastiere, F., Weinmayr, G., Jaensch, A., Nagel, G., Concin, H., Spadaro, J.V., Burnett, R., Chen, H., Szyszkowicz, M., Fann, N., Hubbell, B., Pope, C.A., Apte, J.S., Brauer, M., Cohen, A., Weichenthal, S., Coggins, J., Di, Q., Brunekreef, B., Frostad, J., Lim, S.S., Kan, H., Walker, K.D., Thurston, G.D., Hayes, R.B., Lim, C.C., Turner, M.C., Jerrett, M., Krewski, D., Gapstur, S.M., Diver, W.R., Ostro, B., Goldberg, D., Crouse, D.L., Martin, R.V., Peters, P., Pinault, L., Tjepkema, M., van Donkelaar, A., Villeneuve, P.J., Miller, A.B., Yin, P., Zhou, M., Wang, L., Janssen, N.A.H., Marra, M., Atkinson, R.W., Tsang, H., Quoc Thach, T., Cannon, J.B., Allen, R.T., Hart, J.E., Laden, F., Cesaroni, G., Forastiere, F., Weinmayr, G., Jaensch, A., Nagel, G., Concin, H., Spadaro, J.V., 2018. Global estimates of mortality associated with long-term exposure to outdoor fine particulate matter. *Proc. Natl. Acad. Sci.* 115, 9592–9597. <https://doi.org/10.1073/pnas.1803222115>
- Cao, J., Situ, S., Hao, Y., Xie, S., Li, L., 2022. Enhanced summertime ozone and SOA from biogenic volatile organic compound (BVOC) emissions due to vegetation biomass variability during 1981–2018 in China. *Atmospheric Chem. Phys.* 22, 2351–2364. <https://doi.org/10.5194/acp-22-2351-2022>
- [Chen, X., Wang, X., Wu, X., Guo, J., Zhou, Z., 2021. Influence of roadside vegetation barriers on air quality inside urban street canyons. \*Urban For. Urban Green.\* 63, 127219. <https://doi.org/10.1016/j.ufug.2021.127219>](https://doi.org/10.1016/j.ufug.2021.127219)
- Chowdhury, S., Pozzer, A., Haines, A., Klingmueller, K., Muenzel, T., Paasonen, P., Sharma, A., Venkataraman, C.,

- 813 Lelieveld, J., 2022. Global health burden of ambient PM<sub>2.5</sub> and the contribution of anthropogenic black  
814 carbon and organic aerosols. *Environ. Int.* 159, 107020.
- 815 Cohen, A.J., Brauer, M., Burnett, R., Anderson, H.R., Frostad, J., Estep, K., Balakrishnan, K., Brunekreef, B., Dandona, L.,  
816 Dandona, R., Feigin, V., Freedman, G., Hubbell, B., Jobling, A., Kan, H., Knibbs, L., Liu, Y., Martin, R., Morawska,  
817 L., Pope, C.A., Shin, H., Straif, K., Shaddick, G., Thomas, M., van Dingenen, R., van Donkelaar, A., Vos, T., Murray,  
818 C.J.L., Forouzanfar, M.H., 2017. Estimates and 25-year trends of the global burden of disease attributable to  
819 ambient air pollution: an analysis of data from the Global Burden of Diseases Study 2015. *The Lancet* 389,  
820 1907–1918. [https://doi.org/10.1016/S0140-6736\(17\)30505-6](https://doi.org/10.1016/S0140-6736(17)30505-6)
- 821 [Dunlea, E.J., Herndon, S.C., Nelson, D.D., Volkamer, R.M., San Martini, F., Sheehy, P.M., Zahniser, M.S., Shorter, J.H.,  
822 Wormhoudt, J.C., Lamb, B.K., Allwine, E.J., Gaffney, J.S., Marley, N.A., Grutter, M., Marquez, C., Blanco, S.,  
823 Cardenas, B., Retama, A., Ramos Villegas, C.R., Kolb, C.E., Molina, L.T., Molina, M.J., 2007. Evaluation of nitrogen  
824 dioxide chemiluminescence monitors in a polluted urban environment. \*Atmospheric Chem. Phys.\* 7, 2691–  
825 2704. <https://doi.org/10.5194/acp-7-2691-2007>](#)
- 826 Emery, C., Liu, Z., Russell, A.G., Odman, M.T., Yarwood, G., Kumar, N., 2017. Recommendations on statistics and  
827 benchmarks to assess photochemical model performance. *J. Air Waste Manag. Assoc.* 67, 582–598.  
828 <https://doi.org/10.1080/10962247.2016.1265027>
- 829 Friedl, M., Sulla-Menashe, D., 2019. MCD12Q1 MODIS/Terra+Aqua Land Cover Type Yearly L3 Global 500m SIN Grid  
830 V006. <https://doi.org/10.5067/MODIS/MCD12Q1.006>
- 831 Fuhrer, J., Skärby, L., Ashmore, M.R., 1997. Critical levels for ozone effects on vegetation in Europe. *Environ. Pollut.* 97,  
832 91–106. [https://doi.org/10.1016/S0269-7491\(97\)00067-5](https://doi.org/10.1016/S0269-7491(97)00067-5)
- 833 [Gong, J., Hu, Z., Chen, W., Liu, Y., Wang, J., 2018. Urban expansion dynamics and modes in metropolitan Guangzhou,  
834 China. \*Land Use Policy\* 72, 100–109. <https://doi.org/10.1016/j.landusepol.2017.12.025>](#)
- 835 Guenther, A., Jiang, X., Shah, T., Huang, L., Kemball-Cook, S., Yarwood, G., 2020a. Model of Emissions of Gases and  
836 Aerosol from Nature Version 3 (MEGAN3) for Estimating Biogenic Emissions, in: Mensink, C., Gong, W., Hakami,  
837 A. (Eds.), *Air Pollution Modeling and Its Application XXVI*, Springer Proceedings in Complexity. Springer  
838 International Publishing, Cham, pp. 187–192. [https://doi.org/10.1007/978-3-030-22055-6\\_29](https://doi.org/10.1007/978-3-030-22055-6_29)
- 839 Guenther, A., Jiang, X., Shah, T., Huang, L., Kemball-Cook, S., Yarwood, G., 2020b. Model of Emissions of Gases and  
840 Aerosol from Nature Version 3 (MEGAN3) for Estimating Biogenic Emissions, in: Mensink, C., Gong, W., Hakami,  
841 A. (Eds.), *Air Pollution Modeling and Its Application XXVI*, Springer Proceedings in Complexity. Springer  
842 International Publishing, Cham, pp. 187–192. [https://doi.org/10.1007/978-3-030-22055-6\\_29](https://doi.org/10.1007/978-3-030-22055-6_29)
- 843 Guenther, A.B., Jiang, X., Heald, C.L., Sakulyanontvittaya, T., Duhl, T., Emmons, L.K., Wang, X., 2012a. The Model of  
844 Emissions of Gases and Aerosols from Nature version 2.1 (MEGAN2.1): an extended and updated framework  
845 for modeling biogenic emissions. *Geosci. Model Dev.* 5, 1471–1492. [https://doi.org/10.5194/gmd-5-1471-  
846 2012](https://doi.org/10.5194/gmd-5-1471-2012)
- 847 Guenther, A.B., Jiang, X., Heald, C.L., Sakulyanontvittaya, T., Duhl, T., Emmons, L.K., Wang, X., 2012b. The Model of  
848 Emissions of Gases and Aerosols from Nature version 2.1 (MEGAN2.1): an extended and updated framework  
849 for modeling biogenic emissions. *Geosci. Model Dev.* 5, 1471–1492. [https://doi.org/10.5194/gmd-5-1471-  
850 2012](https://doi.org/10.5194/gmd-5-1471-2012)
- 851 He, C.Q., Zou, Y., Lv, S.J., Flores, R.M., Yan, X.L., Deng, T., Deng, X.J., 2024. The importance of photochemical loss to  
852 source analysis and ozone formation potential: Implications from in-situ observations of volatile organic  
853 compounds (VOCs) in Guangzhou, China. *Atmos. Environ.* 320, 120320.  
854 <https://doi.org/10.1016/j.atmosenv.2023.120320>
- 855 [Jin, S., Guo, J., Wheeler, S., Kan, L., Che, S., Fu, X., Liu, J., Ban-Weiss, G.A., Zhang, J., Huang, X., Ouyang, B., Popoola,  
856 O., Tao, S., Tiwari, A., Kumar, P., Xing, Y., Brimblecombe, P., 2017. Effects of canyon geometry on the  
857 distribution of traffic-related air pollution in a large urban area: Implications of a multi-canyon air pollution  
858 dispersion model. \*Atmos. Environ.\* 165, 111–121. <https://doi.org/10.1016/j.atmosenv.2017.06.031>](#)

- 859 [Jin, S., Guo, J., Wheeler, S., Kan, L., Che, S., Fu, X., Liu, J., Ban-Weiss, G.A., Zhang, J., Huang, X., Ouyang, B., Popoola,](#)  
860 [O., Tao, S., Tiwari, A., Kumar, P., Xing, Y., Brimblecombe, P., 2014. Evaluation of impacts of trees on PM2.5](#)  
861 [dispersion in urban streets. Atmos. Environ. 99, 277–287. <https://doi.org/10.1016/j.atmosenv.2014.10.002>](#)
- 862 [Kai, Z., Wen-jie, Z., Zhi-fang, W., Wei, C., Shao-lin, P., 2011. The influence of urbanization on atmospheric](#)  
863 [environmental quality in Guangzhou, China. 2011 Int. Conf. Electr. Technol. Civ. Eng. ICETCE 3667–3670.](#)  
864 <https://doi.org/10.1109/ICETCE.2011.5776281>
- 865 Le Page, Y., Morton, D., Bond-Lamberty, B., Pereira, J.M.C., Hurtt, G., 2015. HESFIRE: a global fire model to explore the  
866 role of anthropogenic and weather drivers. Biogeosciences 12, 887–903. [https://doi.org/10.5194/bg-12-887-](https://doi.org/10.5194/bg-12-887-2015)  
867 2015
- 868 Lelieveld, J., Klingmüller, K., Pozzer, A., Burnett, R.T., Haines, A., Ramanathan, V., 2019. Effects of fossil fuel and total  
869 anthropogenic emission removal on public health and climate. Proc. Natl. Acad. Sci. 116, 7192–7197.  
870 <https://doi.org/10.1073/pnas.1819989116>
- 871 Lelieveld, J., Pozzer, A., Pöschl, U., Fnais, M., Haines, A., Münzel, T., 2020. Loss of life expectancy from air pollution  
872 compared to other risk factors: a worldwide perspective. Cardiovasc. Res. 116, 1910–1917.
- 873 [Liu, Z., Doherty, R., Wild, O., Hollaway, M., O'Connor, F., 2021. Contrasting chemical environments in summertime for](#)  
874 [atmospheric ozone across major Chinese industrial regions: the effectiveness of emission control strategies.](#)  
875 [Atmospheric Chem. Phys. <https://doi.org/10.5194/ACP-21-10689-2021>](#)
- 876 Lohmann, U., Rotstajn, L., Storelvmo, T., Jones, A., Menon, S., Quaas, J., Ekman, A.M.L., Koch, D., Ruedy, R., 2010. Total  
877 aerosol effect: radiative forcing or radiative flux perturbation? Atmospheric Chem. Phys. 10, 3235–3246.  
878 <https://doi.org/10.5194/acp-10-3235-2010>
- 879 Lombardozi, D., ~~Levis, S.L.~~, Bonan, G., ~~Hess, P.B., Smith, N.G., SparksDukes, J.P., 2014. The InfluenceS., Fisher, R.A.,~~  
880 ~~2015. Temperature acclimation of Chronic Ozone Exposure on Global Carbonphotosynthesis and Water Cycles.~~  
881 ~~J. Clim. 28, 292–305.respiration: A key uncertainty in the carbon cycle-climate feedback. Geophys. Res. Lett.~~  
882 ~~42, 8624–8631. <https://doi.org/10.1029/2015GL065934>~~
- 883 Lu, X., Zhang, L., Wang, X., Gao, M., Li, K., Zhang, Yuzhong, Yue, X., Zhang, Yuanhang, 2020. Rapid Increases in Warm-  
884 Season Surface Ozone and Resulting Health Impact in China Since 2013. Environ. Sci. Technol. Lett. 7, 240–  
885 247. <https://doi.org/10.1021/acs.estlett.0c00171>
- 886 Luecken, D.J., Yarwood, G., Hutzell, W.T., 2019. Multipollutant modeling of ozone, reactive nitrogen and HAPs across  
887 the continental US with CMAQ-CB6. Atmos. Environ. 201, 62–72.  
888 <https://doi.org/10.1016/j.atmosenv.2018.11.060>
- 889 Ma, H., Liang, S., 2022. Development of the GLASS 250-m leaf area index product (version 6) from MODIS data using  
890 the bidirectional LSTM deep learning model. Remote Sens. Environ. 273, 112985.  
891 <https://doi.org/10.1016/j.rse.2022.112985>
- 892 Ma, M., Gao, Y., Ding, A., Su, H., Liao, H., Wang, S., Wang, X., Zhao, B., Zhang, S., Fu, P., Guenther, A.B., Wang, M., Li,  
893 S., Chu, B., Yao, X., Gao, H., 2022. Development and Assessment of a High-Resolution Biogenic Emission  
894 Inventory from Urban Green Spaces in China. Environ. Sci. Technol. 56, 175–184.  
895 <https://doi.org/10.1021/acs.est.1c06170>
- 896 Ma, M., Gao, Y., Wang, Y., Zhang, S., Leung, L.R., Liu, C., Wang, S., Zhao, B., Chang, X., Su, H., Zhang, T., Sheng, L., Yao,  
897 X., Gao, H., 2019. Substantial ozone enhancement over the North China Plain from increased biogenic  
898 emissions due to heat waves and land cover in summer 2017. Atmospheric Chem. Phys. 19, 12195–12207.  
899 <https://doi.org/10.5194/acp-19-12195-2019>
- 900 Masson-Delmotte, V., Zhai, P., Pirani, A., Connors, S.L., Péan, C., Berger, S., Caud, N., Chen, Y., Goldfarb, L., Gomis, M.,  
901 others, 2021. Climate change 2021: the physical science basis. Contrib. Work. Group Sixth Assess. Rep.  
902 Intergov. Panel Clim. Change 2.
- 903 Meng, Y., Song, J., Zeng, L., Zhang, Y., Zhao, Y., Liu, X., Guo, H., Zhong, L., Ou, Y., Zhou, Y., Zhang, T., Yue, D., Lai, S.,  
904 2022. Ambient volatile organic compounds at a receptor site in the Pearl River Delta region: Variations, source

- apportionment and effects on ozone formation. *J. Environ. Sci.* 111, 104–117. <https://doi.org/10.1016/j.jes.2021.02.024>
- Myneni, R., Knyazikhin, Y., Park, T., 2015. MOD15A2H MODIS/Terra leaf area Index/FPAR 8-Day L4 global 500m SIN grid V006. NASA EOSDIS Land Process. DAAC.
- National Centers for Environmental Prediction, National Weather Service, NOAA, U.S. Department of Commerce, 2000. NCEP FNL Operational Model Global Tropospheric Analyses, continuing from July 1999.
- Pye, H.O.T., Murphy, B.N., Xu, L., Ng, N.L., Carlton, A.G., Guo, H., Weber, R., Vasilakos, P., Appel, K.W., Budisulistiorini, S.H., Surratt, J.D., Nenes, A., Hu, W., Jimenez, J.L., Isaacman-VanWertz, G., Misztal, P.K., Goldstein, A.H., 2017. On the implications of aerosol liquid water and phase separation for organic aerosol mass. *Atmospheric Chem. Phys.* 17, 343–369. <https://doi.org/10.5194/acp-17-343-2017>
- Qiu, J., Fang, C., Tian, N., Wang, H., Wang, J., 2023. Impacts of land use and land cover changes on local meteorology and PM<sub>2.5</sub> concentrations in Changchun, Northeast China. *Atmospheric Res.* 289, 106759. <https://doi.org/10.1016/j.atmosres.2023.106759>
- ~~Ramanathan, V., Chung, C., Kim, D., Bettge, T., Buja, L., Kiehl, J.T., Washington, W.M., Fu, Q., Sikka, D.R., Wild, M., 2005. Atmospheric brown clouds: Impacts on South Asian climate and hydrological cycle. *Proc. Natl. Acad. Sci.* 102, 5326–5333. <https://doi.org/10.1073/pnas.0500656102>~~
- Ramanathan, V., Crutzen, P.J., Kiehl, J.T., Rosenfeld, D., Ramanathan, V., Crutzen, P.J., Kiehl, J.T., Rosenfeld, D., 2001. Aerosols, Climate, and the Hydrological Cycle. *Science* 294, 2119–2124. <https://doi.org/10.1126/science.1064034>
- Salamanca, F., Martilli, A., Tewari, M., Chen, F., 2011. A Study of the Urban Boundary Layer Using Different Urban Parameterizations and High-Resolution Urban Canopy Parameters with WRF. *J. Appl. Meteorol. Climatol.* 50, 1107–1128. <https://doi.org/10.1175/2010JAMC2538.1>
- Schlaerth, H.L., Silva, S.J., Li, Y., 2023. Characterizing Ozone Sensitivity to Urban Greening in Los Angeles Under Current Day and Future Anthropogenic Emissions Scenarios. *J. Geophys. Res. Atmospheres* 128, e2023JD039199. <https://doi.org/10.1029/2023JD039199>
- Seinfeld, J.H., Pandis, S.N., Noone, K., 1998. *Atmospheric Chemistry and Physics: From Air Pollution to Climate Change*. *Phys. Today* 51, 88–90. <https://doi.org/10.1063/1.882420>
- Shan, D., Du, Z., Zhang, T., Zhang, X., Cao, G., Liu, Z., Yao, Z., Tang, K., Liang, S., 2023. Variations, sources, and effects on ozone formation of VOCs during ozone episodes in 13 cities in China. *Front. Environ. Sci.* 10, 1084592. <https://doi.org/10.3389/fenvs.2022.1084592>
- Shindell, D., Kuylensstierna, J.C.I., Vignati, E., van Dingenen, R., Amann, M., Klimont, Z., Anenberg, S.C., Müller, N., Janssens-Maenhout, G., Raes, F., Schwartz, J., Faluvegi, G., Pozzoli, L., Kupiainen, K., Höglund-Isaksson, L., Emberson, L., Streets, D., Ramanathan, V., Hicks, K., Oanh, N.T.K., Milly, G., Williams, M., Demkine, V., Fowler, D., Shindell, D., Kuylensstierna, J.C.I., Vignati, E., van Dingenen, R., Amann, M., Klimont, Z., Anenberg, S.C., Müller, N., Janssens-Maenhout, G., Raes, F., Schwartz, J., Faluvegi, G., Pozzoli, L., Kupiainen, K., Höglund-Isaksson, L., Emberson, L., Streets, D., Ramanathan, V., Hicks, K., Oanh, N.T.K., Milly, G., Williams, M., Demkine, V., Fowler, D., Shindell, D., Kuylensstierna, J.C.I., Vignati, E., van Dingenen, R., Amann, M., Klimont, Z., Anenberg, S.C., Müller, N., Janssens-Maenhout, G., Raes, F., Schwartz, J., Faluvegi, G., Pozzoli, L., Kupiainen, K., Höglund-Isaksson, L., Emberson, L., Streets, D., Ramanathan, V., Hicks, K., Oanh, N.T.K., Milly, G., Williams, M., Demkine, V., Fowler, D., 2012. Simultaneously Mitigating Near-Term Climate Change and Improving Human Health and Food Security. *Science* 335, 183–189. <https://doi.org/10.1126/science.1210026>
- ~~Sindelarova, K., Granier, C., Bouarar, I., Guenther, A., Tilmes, S., Stavrou, T., Müller, J.-F., Kuhn, U., Stefani, P., Knorr, W., 2014. Global data set of biogenic VOC emissions calculated by the MEGAN model over the last 30 years. *Atmospheric Chem. Phys.* 14, 9317–9341. <https://doi.org/10.5194/acp-14-9317-2014>~~
- Soleimanian, E., Wang, Y., Li, W., Liu, X., Griggs, T., Flynn, J., Walter, P.J., Estes, M.J., 2023. Understanding ozone episodes during the TRACER-AQ campaign in Houston, Texas: The role of transport and ozone production

- sensitivity to precursors. *Sci. Total Environ.* 900, 165881. <https://doi.org/10.1016/j.scitotenv.2023.165881>
- Solomon, S., 2007. *Climate change 2007-the physical science basis: Working group I contribution to the fourth assessment report of the IPCC*. Cambridge university press.
- [Tiwari, A., Kumar, P., 2020. Integrated dispersion-deposition modelling for air pollutant reduction via green infrastructure at an urban scale. \*Sci. Total Environ.\* 723, 138078. <https://doi.org/10.1016/j.scitotenv.2020.138078>](#)
- [Tomson, M., Kumar, P., Barwise, Y., Perez, P., Forehead, H., French, K., Morawska, L., Watts, J.F., 2021. Green infrastructure for air quality improvement in street canyons. \*Environ. Int.\* 146, 106288. <https://doi.org/10.1016/j.envint.2020.106288>](#)
- Wang, H., Liu, Z., Wu, K., Qiu, J., Zhang, Y., Ye, B., He, M., 2022. Impact of Urbanization on Meteorology and Air Quality in Chengdu, a Basin City of Southwestern China. *Front. Ecol. Evol.* 10, 845801. <https://doi.org/10.3389/fevo.2022.845801>
- Wang, H., Liu, Z., Zhang, Y., Yu, Z., Chen, C., 2021. Impact of different urban canopy models on air quality simulation in Chengdu, southwestern China. *Atmos. Environ.* 267, 118775. <https://doi.org/10.1016/j.atmosenv.2021.118775>
- Wang, N., Lyu, X., Deng, X., Huang, X., Jiang, F., Ding, A., 2019a. Role of vegetation in deposition and dispersion of air pollution in urban parks. *Atmos. Environ.* 201, 73–83. <https://doi.org/10.1016/j.atmosenv.2018.12.027>
- [Wang, N., Lyu, X., Deng, X., Huang, X., Jiang, F., Ding, A., 2019b. Aggravating O3 pollution due to NOx emission control in eastern China. \*Sci. Total Environ.\* 677, 732–744. <https://doi.org/10.1016/j.scitotenv.2019.04.388>](#)
- [Wang, P., Chen, Y., Hu, J., Zhang, H., Ying, Q., 2019. Attribution of Tropospheric Ozone to NOx and VOC Emissions: Considering Ozone Formation in the Transition Regime. \*Environ. Sci. Technol.\* 53, 1404–1412. <https://doi.org/10.1021/acs.est.8b05981>](#)
- WHO, 2021. WHO global air quality guidelines: particulate matter (PM2.5 and PM10), ozone, nitrogen dioxide, sulfur dioxide and carbon monoxide. World Health Organization.
- Wu, K., Yang, X., Chen, D., Gu, S., Lu, Y., Jiang, Q., Wang, K., Ou, Y., Qian, Y., Shao, P., Lu, S., 2020. Estimation of biogenic VOC emissions and their corresponding impact on ozone and secondary organic aerosol formation in China. *Atmospheric Res.* 231, 104656. <https://doi.org/10.1016/j.atmosres.2019.104656>
- [Yang, H., Chen, T., Lin, Y., Buccolieri, R., Mattsson, M., Zhang, M., Hang, J., Wang, Q., 2020. Integrated impacts of tree planting and street aspect ratios on CO dispersion and personal exposure in full-scale street canyons. \*Build. Environ.\* 169, 106529. <https://doi.org/10.1016/j.buildenv.2019.106529>](#)
- Yao, Z., Huang, G., 2023. Effects of Land Use Changes Across Different Urbanization Periods on Summer Rainfall in the Pearl River Delta Core Area. *Int. J. Disaster Risk Sci.* 14, 458–474. <https://doi.org/10.1007/s13753-023-00497-8>
- Yim, S.H.L., Wang, M., Gu, Y., Yang, Y., Dong, G., Li, Q., 2019. Effect of Urbanization on Ozone and Resultant Health Effects in the Pearl River Delta Region of China. *J. Geophys. Res. Atmospheres* 124, 11568–11579. <https://doi.org/10.1029/2019JD030562>
- [Zhao, Y., Xi, M., Zhang, Q., Dong, Z., Ma, M., Zhou, K., Xu, W., Xing, J., Zheng, B., Wen, Z., Liu, X., Nielsen, C.P., Liu, Y., Pan, Y., Zhang, L., 2022. Decline in bulk deposition of air pollutants in China lags behind reductions in emissions. \*Nat. Geosci.\* 15, 190–195. <https://doi.org/10.1038/s41561-022-00899-1>](#)
- [Zhang, Y., Cao, F., 2015. Fine particulate matter \(PM2.5\) in China at a city level. \*Sci. Rep.\* 5, 14884.](#)
- Zheng, J., Shao, M., Che, W., Zhang, L., Zhong, L., Zhang, Y., Streets, D., 2009. Speciated VOC Emission Inventory and Spatial Patterns of Ozone Formation Potential in the Pearl River Delta, China. *Environ. Sci. Technol.* 43, 8580–8586. <https://doi.org/10.1021/es901688e>
- Zhou, D., Zhao, S., Zhang, L., Sun, G., Liu, Y., 2015. The footprint of urban heat island effect in China. *Sci. Rep.* 5, 11160.